The FEBS Journal

FEBS PRESS science publishing by scientists

Mechanisms to reduce the cytotoxicity of pharmacological nicotinamide concentrations in the pathogenic fungus *Candida albicans*

Rahul Ghugari[1,2], Sarah Tsao[1], Mark Schmidt[3], Éric Bonneil[1], Charles Brenner[4] and Alain Verreault[1,5]

1 Institute for Research in Immunology and Cancer, Université de Montréal, QC, Canada
2 Programme de Biologie Moléculaire, Université de Montréal, QC, Canada
3 Department of Biochemistry, Carver College of Medicine, University of Iowa, IA, USA
4 Department of Diabetes & Cancer Metabolism, Beckman Research Institute, City of Hope National Medical Center, Duarte, CA, USA
5 Département de Pathologie et Biologie Cellulaire, Université de Montréal, QC, Canada

Keywords
Candida albicans; H3K56 hyperacetylation; NAM exchange reaction; nicotinamide cytotoxicity; pathogenic fungi; pharmacological nicotinamide concentration; sirtuin Hst3; sirtuin inhibition; supraphysiological nicotinamide concentration; vitamin B_3

Correspondence
A. Verreault, Institute for Research in Immunology and Cancer (IRIC), Université de Montréal, P.O. Box 6128, Station Centre-Ville, Montreal, QC, Canada H3C 3J7
Tel: +1 514 706 9667
E-mail: alain.verreault@umontreal.ca
IRIC Web site: https://www.iric.ca/en/

Ghugari Rahul and Tsao Sarah contributed equally to this work

(Received 13 April 2020, revised 13 September 2020, accepted 4 November 2020)

doi:10.1111/febs.15622

Candida albicans is a pathogenic fungus that causes systemic infections and mortality in immunosuppressed individuals. We previously showed that deacetylation of histone H3 lysine 56 by Hst3 is essential for *C. albicans* viability. Hst3 is a fungal-specific NAD^+-dependent protein deacetylase of the sirtuin family. *In vivo*, supraphysiological concentrations of nicotinamide (NAM) are required for Hst3 inhibition and cytotoxicity. This underscores the importance of identifying mechanisms by which *C. albicans* can modulate intracellular NAM concentrations. For the first time in a pathogenic fungus, we combine genetics, heavy isotope labeling, and targeted quantitative metabolomics to identify genes, pathways, and mechanisms by which *C. albicans* can reduce the cytotoxicity of high NAM concentrations. We discovered three distinct fates for supraphysiological NAM concentrations. First, upon transient exposure to NAM, high intracellular NAM concentrations rapidly return near the physiological levels observed in cells that are not exposed to NAM. Second, during the first step of a fungal-specific NAM salvage pathway, NAM is converted into nicotinic acid, a metabolite that cannot inhibit the sirtuin Hst3. Third, we provide evidence that NAM enters the NAD^+ metabolome through a NAM exchange reaction that contributes to NAM-mediated inhibition of sirtuins. However, in contrast to the other fates of NAM, the NAM exchange reaction cannot cause a net decrease in the intracellular concentration of NAM. Therefore, this reaction cannot enhance resistance to NAM. In summary, we demonstrate that *C. albicans* possesses at least two mechanisms to attenuate the cytotoxicity of pharmacological NAM

Abbreviations
AMP, adenosine monophosphate; bp, base pair(s); Ca, *Candida albicans*; CGD, *Candida* Genome Database; CRISPR, clustered regularly interspaced short palindromic repeats; Dox, doxycycline; gDNA, genomic DNA; GRACE, gene replacement and conditional expression; H3K56, histone H3 lysine 56 (nonacetylated); H3K56ac, histone H3 acetylated at lysine 56; HEPES, 4-(2-hydroxyethyl)-1-piperazine ethanesulfonic acid; HIV, human immunodeficiency virus; hNAM, heavy NAM or tetradeuterated [2, 4, 5, 6] d_4-nicotinamide; ICU, intensive care unit; Ipp1, inorganic pyrophosphatase 1; isoNAM, isonicotinamide; kb, kilobase (1000 nucleotides); LC-MS/MS, liquid chromatography coupled to tandem mass spectrometry; MMS, methyl methanesulfonate; MS, mass spectrometry; NA, nicotinic acid; NaAD, nicotinic acid adenine dinucleotide; NAD^+, nicotinamide adenine dinucleotide; NAM, nicotinamide; NAMN, nicotinic acid mononucleotide; NMN, nicotinamide mononucleotide; Npt1, nicotinic acid phosphoribosyltransferase; NR, nicotinamide riboside; Nrk1, nicotinamide riboside kinase; PCR, polymerase chain reaction; Pi, inorganic phosphate; PPi, inorganic pyrophosphate; Sc, *Saccharomyces* cerevisiae; SC, synthetic complete medium; SD, standard deviation; SRM, selected reaction monitoring; WT, wild-type.

concentrations. It seems likely that those two mechanisms of resistance to cytotoxic NAM concentrations are conserved in many other pathogenic fungi.

Introduction

Candida albicans is an opportunistic pathogen that normally resides in the mouth, throat, and gastrointestinal and urogenital tracts of healthy individuals. *C. albicans* causes vulvovaginal infections that are not life-threatening, but nonetheless very painful and often recurrent [1–4]. In addition, *C. albicans* can provoke oropharyngeal infections or systemic infections in immunocompromised individuals suffering from AIDS, and systemic infections in patients treated with cancer chemotherapeutic agents that cripple the immune system or patients deliberately immunosuppressed in preparation for hematopoïetic stem cell or solid organ transplantation [1–4]. In patients with crippled immunity, systemic dissemination and invasion of vital organs by *C. albicans* can result in significant morbidity and mortality [1,2]. Cases of invasive fungal infections have steadily increased over time due to an increasing number of patients needing cancer chemotherapy and/or hematopoïetic stem cell transplantation [5,6]. Invasive *C. albicans* infections are the most common cause of bloodstream infections in the United States after bacterial infections caused by *Staphylococcal* and *Enterococcal* species [1,7]. In immunocompromised patients, mortality rates that result from invasive *C. albicans* infections can reach as much as 40% [8].

The repertoire of therapeutic antifungal agents is rather limited. Only four chemically distinct classes of therapeutic agents are commonly employed to treat invasive fungal infections: flucytosine, polyenes, azoles, and echinocandins. Unfortunately, all those classes of antifungal drugs suffer from limitations [9]. For instance, azoles are the most frequently used drugs to treat fungal infections because they are administered orally and some azole compounds are relatively inexpensive. The low cost of some azole family members is particularly salient in developing countries where infections by *C. albicans* and other fungal pathogens are widespread. Unfortunately, the emergence of azole-resistant strains is facilitated by the fact that azoles are cytostatic, rather than cytocidal.

A number of studies indicate that covalent modifications of histone proteins, the foundation stones of chromatin, exert a major influence on the virulence of pathogenic fungi. Notably, compelling evidence indicates that mutations that cripple th of histone acetyltransferases and histone deacetylases attenuate fungal virulence [10–14]. Therefore, targeting enzymes that covalently modify histones represents a novel, and poorly explored therapeutic strategy [9,15–17]. In *C. albicans,* perturbation of histone H3 lysine 56 acetylation (H3K56ac) affects virulence and viability [10,11]. Histone H3K56 is acetylated by Rtt109 [18–21] and deacetylated by Hst3 [22–25], two enzymes with fungal-specific properties that are conserved in essentially all the known pathogenic fungi including the multidrug-resistant and highly pathogenic species *Candida auris* [26]. While there were worthwhile efforts to screen for small molecules that inhibit Rtt109 [27,28], we provided evidence that inhibition of Hst3, the *C. albicans* enzyme that deacetylates H3K56, was also an appealing strategy to uncover novel antifungal agents [11]. Hst3 is a member of the sirtuin family of deacetylases that require nicotinamide adenine dinucleotide (NAD^+) as substrate [24,25]. During the deacetylation reaction, an acetyl group is transferred from the protein substrate to the ADP-ribose moiety of NAD^+, leading to the release of free NAM (Fig. 9A). In turn, NAM is a relatively weak inhibitor of the deacetylase activities of Hst3 [25] and other sirtuins [29–31]. When *C. albicans* cells are exposed to supraphysiological concentrations of NAM (0.8–1.6 mM), Hst3 inhibition results in hyperacetylation of H3K56 and cytotoxicity [11]. Furthermore, high concentrations of NAM reduce fungal invasion of the kidneys and the heart, and attenuate the virulence of *C. albicans* during systemic infections of immunocompromised mice [11].

Nicotinamide meets some of the key criteria required of an effective antifungal agent [32]. First, it exhibits a broad spectrum of antifungal activity. For instance, NAM inhibits the proliferation of azole- or echinocandin-resistant clinical isolates of *C. albicans*, other *Candida* species, and even *Aspergillus fumigatus* [11]. Second, the antifungal properties of NAM are exerted, in large part, through inhibition of Hst3, a sirtuin with fungal-specific properties that is essential for *C. albicans* viability [11]. Third, unlike echinocandins, NAM can be administered orally. Fourth, NAM is Food and Drug Administration-approved as a food

supplement and clinical trials to assess its therapeutic potential to treat a number of human conditions demonstrated that oral administration of daily doses as high as 3–6 grams of NAM over the course of several weeks did not result in major side effects [33–36]. One of the reasons why NAM is well tolerated in humans stems from the fact that, as a form of vitamin B_3, NAM is incorporated into NAD^+ through enzymatic steps catalyzed by NAM phosphoribosyltransferase (NAMPT) and nicotinamide mononucleotide adenylyltransferase (NMNAT), two enzymes that are ubiquitously expressed in human tissues [37]. Owing to differences in the experimental procedures and instrumentation employed to determine NAM concentrations in circulation, the results of several pharmacokinetic studies are difficult to compare with each other [35,36,38–40]. In one pharmacokinetic study, peak concentrations of NAM in circulation ranged from 0.8 to 2.3 mM with a median half-life of 9.3 h [41]. Those NAM concentrations were fungicidal and attenuated virulence in an immunocompromised mouse model of systemic *C. albicans* infections [11]. With the caveat that promising results in mice do not necessarily presage therapeutic efficacy in humans, these results suggest that, despite the need to maintain elevated concentrations in circulation, NAM may prove a potentially valuable new weapon in the arsenal to fight fungal infections.

Physiological NAM concentrations in *C. albicans* range from 25 μM up to ~ 75 μM. In contrast, pharmacological concentrations of NAM that are cytocidal to *C. albicans* range from 800 to 1600 μM *in vitro* [11]. Throughout this manuscript, we use the term 'pharmacological NAM concentrations' to refer to supraphysiological concentrations that are sufficiently high to be cytocidal to *C. albicans in vitro* and in a mouse model of systemic infections [11]. The purpose of this study was to uncover mechanisms that reduce the abundance of intracellular NAM in *C. albicans,* and thereby attenuate the cytotoxicity of pharmacological NAM concentrations.

We demonstrate that NAM has at least three distinct fates in *C. albicans*. First, upon transient exposure to pharmacological NAM concentrations, most intracellular NAM comes out of *C. albicans* cells. The second mechanism that contributes to reduce the abundance of intracellular NAM is its incorporation into NAD^+ that occurs through a NAM recycling pathway that is conserved among many fungal species, but does not exist in humans. In this pathway, NAM deamidation by the nicotinamidase Pnc1 produces nicotinic acid (NA), which then serves as substrate to generate NAD^+ through the classical Preiss–Handler pathway [42]. NA formed during the first step of the pathway cannot inhibit Hst3 or other sirtuins. Third, we show that NAM enters the NAD^+ metabolome through a NAM exchange reaction that involves NAM-mediated inhibition of sirtuins. However, in contrast to the other mechanisms, the NAM exchange reaction cannot lead to a net decrease in the intracellular abundance of NAM. Therefore, this reaction cannot contribute to *C. albicans* resistance to pharmacological NAM concentrations.

Results

Pathways for NAD^+ synthesis in *Candida albicans*

In *Saccharomyces cerevisiae*, the first step of NAM salvage to generate NAD^+ is its deamidation by the nicotinamidase Pnc1 (Fig. 1, reaction **1**) 851371541 [42]. This reaction generates NA [43] that, in turn, serves as precursor for biosynthesis of NAD^+ through the canonical pathway for NA salvage in fungi, known as the Preiss–Handler pathway (Fig. 1, reactions **2, 3a and 4**) [42]. The nicotinamidase and the enzymes that catalyze the Preiss–Handler pathway for NA salvage clearly exist in the NAD^+ auxotroph *Candida glabrata* in which *de novo* synthesis of NAD^+ from tryptophan (Trp) through the so-called kynurenine pathway (Fig. 1, reactions leading from Trp to NAD^+) is blocked by a mutation [44]. Based on evolutionary conservation of the enzymes, the Preiss–Handler pathway exists in many other pathogenic fungi [45].

Using either [*carbonyl*-^{14}C] NAM or [5-^{3}H] Trp, Jacobson and colleagues demonstrated that *C. albicans* possesses a NAM salvage pathway to generate NAD^+ and a kynurenine pathway for *de novo* synthesis of NAD^+ from Trp [46], but the genes and enzymes involved were not known. We found that the *C. albicans* genome encodes all the enzymes involved in the kynurenine pathway for *de novo* synthesis of NAD^+ from Trp (Fig. 1, Bna2, Bna4, Bna5, Bna1, Bna6, Nma1, and Qns1) [47]. Likewise, the enzymes necessary to salvage NA through the classical Preiss–Handler pathway [42] (Fig. 1, Npt1, Nma1, and Qns1) and the enzymes needed to salvage nicotinamide riboside (NR) [48] (Fig. 1, Nrk1 and Nma1) are all encoded in the *C. albicans* genome.

The *Candida albicans* nicotinamidase Pnc1

A sequence homology search identified a single gene that likely encodes the nicotinamidase Pnc1 [43], an enzyme necessary to convert NAM into NA (Fig. 1, reaction **1**), which is then salvaged to generate NAD^+

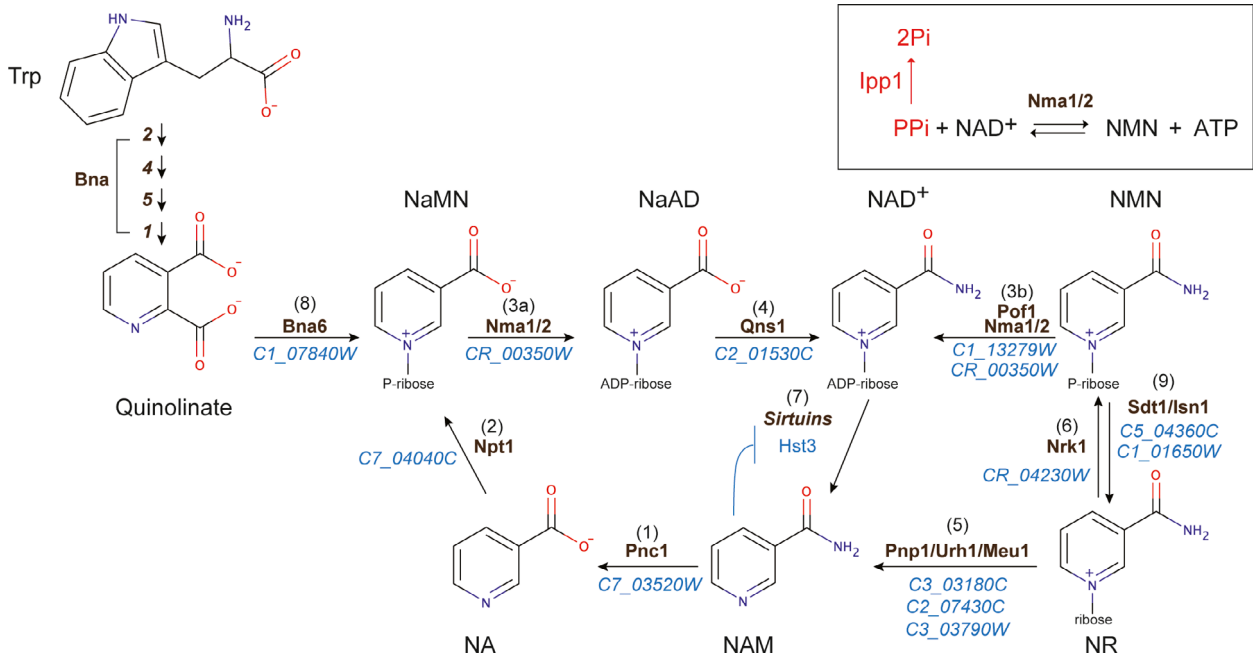

Fig. 1. Enzymes involved in yeast NAM and NAD^+ metabolism. *S. cerevisiae* enzymes are listed above the arrows and numbered. *C. albicans* genes that encode sequence homologues of *S. cerevisiae* enzymes are indicated in blue below the arrows. In *S. cerevisiae*, NAD^+ can be synthesized via three pathways: a *de novo* pathway and two salvage pathways that recycle the different forms of vitamin B_3 known as NAM, NA, and NR. The first portion of the *de novo* pathway, also known as the kynurenine pathway, converts tryptophan (Trp) through a series of reactions catalyzed by Bna enzymes, culminating in Bna6-catalyzed formation of NaMN **(8)**. The Preiss–Handler salvage pathway recycles NAM and NA to produce NAD^+. The first step is the deamidation of NAM to produce NA, a reaction catalyzed by the nicotinamidase Pnc1 **(1)**. This is followed by conversion of NA into NaMN catalyzed by Npt1 **(2)**. The *de novo* and canonical salvage pathways merge at NaMN and subsequently share two reactions. Adenylation of NaMN catalyzed by either Nma1 or Nma2 in *S. cerevisiae* produces NaAD **(3a)**. Second, amidation of NaAD generates NAD^+**(4)** through a reaction catalyzed by the NAD^+ synthetase Qns1. The NR salvage pathway starts by conversion of NR into NMN, a reaction catalyzed by the NR kinase Nrk1 **(6)**. This is followed by adenylation of NMN to produce NAD^+, which is catalyzed by Nma1, Nma2 or Pof1 in *S. cerevisiae***(3b)**. Alternatively, conversion of NR into NAM by the nucleosidase Urh1 or the phosphorylases Pnp1 and, to a lesser extent Meu1 **(5)**, provides a conduit for the NAM moiety of NR to enter the Preiss–Handler salvage pathway described above for NAM and NA. The 5′-nucleotidases Sdt1 and Isn1 hydrolyze the phosphate group of NMN to generate the nucleoside NR **(9)**. Sirtuins such as Hst3 **(7)** require NAD^+ as a substrate to deacetylate proteins, and one of their reaction products is NAM. NAM can also act as a sirtuin inhibitor through the so-called NAM reaction. Rectangular inset: Adenylation of NMN by Nma1 or Nma2 to produce NAD^+ is a readily reversible reaction *in vitro*. However, *in vivo* the synthesis of NAD^+ by Nma1 or Nma2 is largely irreversible. This is because the synthesis of NAD^+ also generates a molecule of PPi, whose hydrolysis by inorganic pyrophosphatase (Ipp1) is a reaction that is highly favorable energetically.

through the Preiss–Handler pathway (Fig. 1, reactions **2**, **3a,** and **4**).

Overall, *C. albicans* Pnc1 shares a considerable degree of amino acid sequence similarity with *S. cerevisiae* Pnc1, and the *C. albicans* enzyme also possesses a triad of catalytic residues that are crucial for the deamidase activity of nicotinamidases (Fig. 2, asterisks above the ScPnc1 sequence) [49].

Because NAM can inhibit sirtuins, but NA does not, our initial hypothesis was that Pnc1 might reduce the cytotoxicity of pharmacological NAM concentrations by rapidly converting NAM into NA. This working hypothesis predicted that, when exposed to NAM, cells lacking Pnc1 would accumulate considerably higher amounts of NAM than wild-type (WT) cells, and the resulting inhibition of the sirtuin Hst3 would cause hyperacetylation of H3K56 and cytotoxicity. To test this hypothesis, we generated a *C. albicans* homozygous null mutant that lacks Pnc1. This mutant, hereafter referred to as *pnc1*Δ/Δ, was created by replacing the two alleles of the *PNC1* gene by *HIS1* and *ARG4* auxotrophic markers [50]. WT and *pnc1*Δ/Δ cells were grown in liquid cultures of synthetic complete medium lacking niacin (SC-Niacin: a culture medium that lacks NAM, NA, and NR based on our mass spectrometry data), supplemented with increasing concentrations of NAM. We found that *pnc1*Δ/Δ cells are, at best, mildly sensitive to NAM compared with

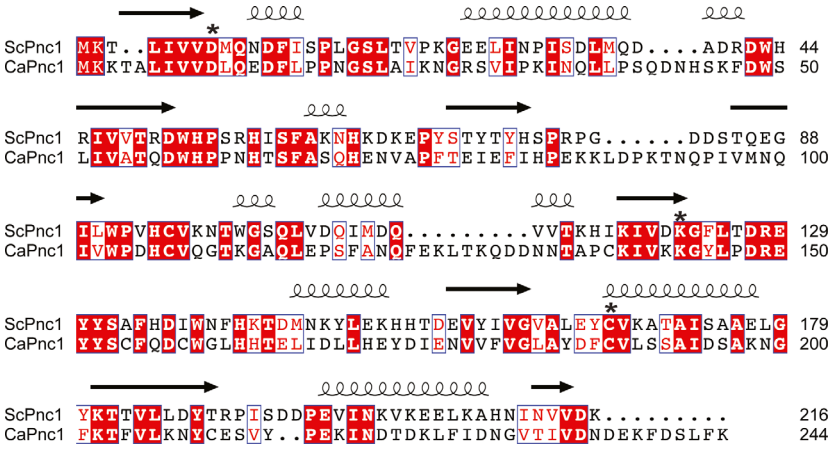

Fig. 2. Structure-based sequence alignment of *S. cerevisiae* and *C. albicans* Pnc1. Secondary structure-based protein alignment of *S. cerevisiae* Pnc1 with a potential homologue of Pnc1 (C7_03520w) in *C. albicans*. The alignment was obtained using ClustalW modified to exploit structural data from *S. cerevisiae* Pnc1 (PDB 2H0R) using ESPript [94]. Identical residues are boxed and highlighted in white over a red background. Conversely, homologous residues are boxed and depicted in red over a light gray background. Conserved residues that form the catalytic triad of *S. cerevisiae* Pnc1 (*), α-helices (spirals), and β-strands (arrows) are indicated above the ScPnc1 sequence.

WT cells (Fig. 3A, empty circles versus black triangles). The mild NAM sensitivity of cells lacking Pnc1 was only discernible over a narrow range of concentrations that spanned from ~ 0.4 to 1.6 mM NAM (Fig. 3B, empty circles versus black triangles).

Given the activity of Pnc1 in converting NAM into NA, these results seem counter-intuitive but, in fact, they can be readily explained by the experimental procedure that we employed. Our experiments involved continuous exposure of *C. albicans* to culture media containing up to 4 mM NAM (Fig. 3B) or 10 mM NAM (Fig. 3A), and the volume of culture medium containing these high NAM concentrations was far greater than the total intracellular volume of all the cells in each culture. Under these conditions, even WT cells that express Pnc1 cannot substantially reduce the intracellular concentration of NAM because, as soon as NAM molecules are converted into NA by Pnc1, the vast excess of extracellular NAM molecules replenish intracellular NAM to its high concentration. When Pnc1 is continuously saturated by NAM, cells expressing WT Pnc1 and cells lacking Pnc1 both experience very similar intracellular NAM concentrations and, therefore, *pnc1*Δ/Δ cells are not more sensitive to NAM than WT cells (Fig. 3A). We suggest that Pnc1 is not fully saturated at moderate extracellular NAM concentrations (0.4–1.2 mM NAM, Fig. 3B) and therefore capable of reducing the intracellular NAM concentration to a modest extent because the influx of NAM molecules from the medium likely occurs less efficiently than in the presence of 10 mM NAM. Consistent with this interpretation, when the extracellular NAM concentration was moderate, two independent *pnc1*Δ/Δ isolates were found slightly more sensitive to NAM than WT cells (Fig. 3B, empty circles). In contrast to WT and *pnc1*Δ/Δ cells, *rtt109*Δ/Δ mutants were resistant to NAM over a broad range of concentrations (Fig. 3A, empty squares). Because cells lacking Rtt109 cannot acetylate H3K56 [10,11], the considerable resistance to NAM of *rtt109*Δ/Δ mutants suggests that the cytotoxicity of NAM in WT cells is dependent, at least in part, on hyperacetylation of H3K56.

We observed that the *PNC1* mRNA increases in abundance when WT cells are treated with the alkylating agent methyl methanesulfonate (MMS, data not shown). This suggests that the demand for Pnc1-mediated conversion of NAM into NA may be enhanced in response to MMS-induced lesions. We felt that this was potentially of interest because we previously showed that inhibition of Hst3 by NAM causes extensive DNA damage and enhances sensitivity to MMS [11]. Based on the above, it seemed formally possible that an MMS-induced increase in Pnc1-mediated conversion of NAM into NA might mitigate the DNA damage and cytotoxicity caused by Hst3 inhibition. However, this hypothesis proved incorrect because mutant cells lacking Pnc1 were as sensitive to MMS as WT cells (Fig. 3C, empty circles versus black triangles).

We constructed two independent *PNC1* revertants (*pnc1*Δ/Δ+ *PNC1* #1 and #2 in Fig. 3B) in which one

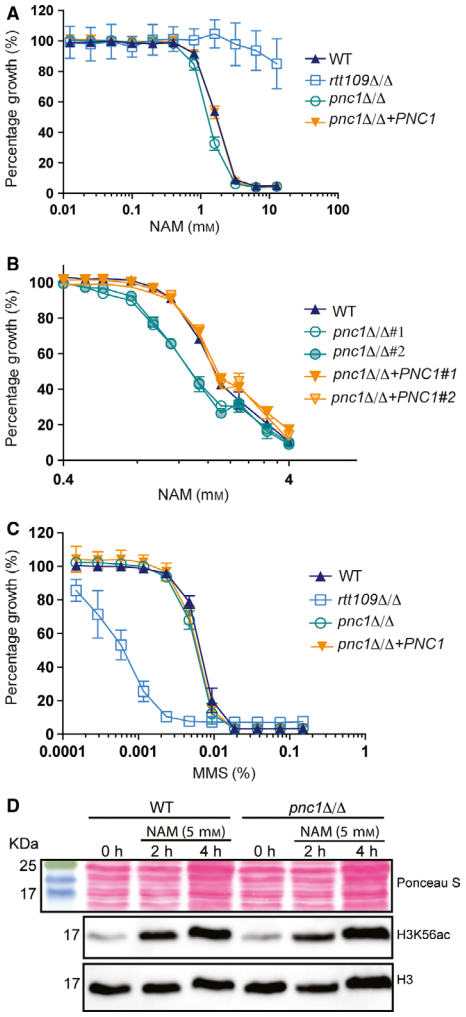

Fig. 3. Cells lacking Pnc1 are mildly more sensitive to NAM than WT cells, but *pnc1* null mutants and WT cells are equally sensitive to MMS. (A-C) Growth inhibition assays in liquid cultures. Strains were grown at 30 °C for 24 h in SC-Niacin medium containing increasing concentrations of either NAM (A, B) or MMS (C) prior to measuring the optical density at 595 nm (OD595). The percentage growth is the ratio of OD595 values in wells containing either NAM or MMS over the OD595 values of control wells lacking those chemicals. Strains labeled #1 and #2 are two independent isolates of the same strain. Panel 3A (supraphysiological NAM concentrations): The error bars represent the SD from the mean of either nine (WT, *rtt109*Δ/Δ and *pnc1*Δ/Δ) or six biological replicates (*pnc1*Δ/Δ + *PNC1* revertant). Please note that the means of the nine replicates for WT, *rtt109*Δ/Δ, and *pnc1*Δ/Δ cells were derived from three independent experiments, each performed as three biological replicates for Figs. 3A, 5B, and 7A (see Supplementary Tables for the raw data). As a result, the curves for WT, *rtt109*Δ/Δ, and *pnc1*Δ/Δ cells are identical in Figs 3A, 5B, and 7A. Panel 3B (moderate NAM concentrations): The error bars represent the SD from the mean of three biological replicates for each of the five strains. Panle C (MMS sensitivity): The error bars represent the SD from the mean of six biological replicates for each of the four strains. (D) WT cells and *pnc1*Δ/Δ mutants grown in SC-Niacin were exposed to 5 mM NAM for 0 h (aliquots of cells were harvested prior to the addition of NAM), 2 or 4 h at 30 °C. Whole-cell lysates were analyzed by immunoblotting with antibodies against K56-acetylated histone H3 (H3K56ac) or nonmodified H3 as loading control. Ponceau S staining of the nitrocellulose membrane served as a second loading control. Panel D shows a representative result from two independent experiments.

copy of the WT *PNC1* gene was re-introduced at its original locus to generate heterozygous *pnc1*Δ/*PNC1* strains. This restored NAM resistance to a level comparable to that observed in WT cells (Fig. 3B, yellow triangles). This shows that the mild NAM sensitivity of *pnc1*Δ/Δ cells is truly dependent upon the absence of *PNC1*, rather than other genetic alterations that might have arisen during strain construction. The mild sensitivity of *pnc1*Δ/Δ cells is in keeping with the fact that, when continuously exposed to 5 mM NAM for up to 4 h, cells lacking Pnc1 do not show higher levels of histone H3K56 acetylation than WT cells (Fig. 3D).

Pnc1 is the sole nicotinamidase in *C. albicans*

The mild NAM sensitivity of *pnc1*Δ/Δ cells was counter-intuitive but, as described earlier, can be largely explained by our experimental design. However, a nonmutually exclusive possibility that may contribute to the mild NAM sensitivity of *pnc1*Δ/Δ cells is that deamidases that normally act on substrates other than NAM might compensate for the absence of Pnc1 by converting NAM into NA, a metabolite that cannot inhibit sirtuins. To address this possibility, *pnc1*Δ/Δ mutants and WT cells were continuously exposed to 5 mM NAM for up to 120 min, and the abundance of NAM and NAD^+-related metabolites determined as a function of time. To determine metabolite concentrations, we took advantage of a method previously optimized for extraction of NAD^+-related metabolites, combined with quantitative and targeted analysis of the *S. cerevisiae* NAD^+ metabolome by liquid chromatography coupled to tandem mass spectrometry (LC-MS/MS) [51]. Cells were initially grown in SC-Niacin, a medium lacking the three forms of vitamin B_3: NA, NAM, and NR. Within 7 min after addition of 5 mM NAM, we observed a sharp increase in NAM concentrations from ≈ 50 μM up to > 1.75 mM in WT (SN152) cells, *pnc1*Δ/Δ mutants and *pnc1*Δ /*pnc1*Δ + *PNC1* revertant cells (Fig. 4A). In parallel, the intracellular concentration of NA rose rapidly (within

< 7 min) in WT (SN152) and, to a lesser extent, in *PNC1* revertant cells (Fig. 4B). *PNC1* revertant cells are heterozygous and, consistent with this, NA concentrations were lower in *PNC1* revertants than in WT cells throughout the time course from 7 up to 120 min (Fig. 4B). In striking contrast to WT and *PNC1* revertant cells, NA was below our limit of detection in *pnc1*Δ/Δ cells even after 120 min in the continuous presence of 5 mM NAM (n.d. in Fig. 4B). This result indicates that, even when exposed to high NAM concentrations, *pnc1*Δ/Δ mutants cannot convert NAM into NA, which strongly suggests that Pnc1 is the only enzyme that can deamidate NAM to generate NA in *C. albicans*.

NAM efflux

In order to cause extensive DNA damage, NAM must be sufficiently abundant to inhibit Hst3 during the course of 2–3 cell division cycles (2–3 h at 30 °C) [11]. Given this, we sought to determine the rate at which the NAM concentration decreased following its complete removal from cell cultures. For this purpose, we designed a procedure to measure intracellular metabolite concentrations after transient exposure to NAM (Materials and methods). Cultures of WT (SN152), *pnc1*Δ/Δ, and *npt1*Δ/Δ cells in SC-Niacin medium were continuously exposed to NAM for 7 min. To remove extracellular NAM, the cultures were subjected to filtration under vacuum through 0.45 µ membranes [52], which retains yeast cells but removes the culture medium containing 5 mM NAM. For each culture, extensive washes of the 0.45 µ membranes were performed with phosphate-buffered saline (200 mL PBS) to remove extracellular NAM molecules that might have simply adhered nonspecifically to the membranes and/or to the surface of cells. The membranes coated with cells were transferred to a beaker containing SC-Niacin medium lacking NAM. After 1 min over a shaking platform, the vast majority of cells had detached from the membranes. A first aliquot of the cell suspension was collected as soon as possible after the cells had been transferred to SC-Niacin (3-min time point in Fig. 4D, corresponding to 2 min of filtration and washes, followed by 1 min in SC-Niacin to detach cells from the membrane). The second aliquot was collected

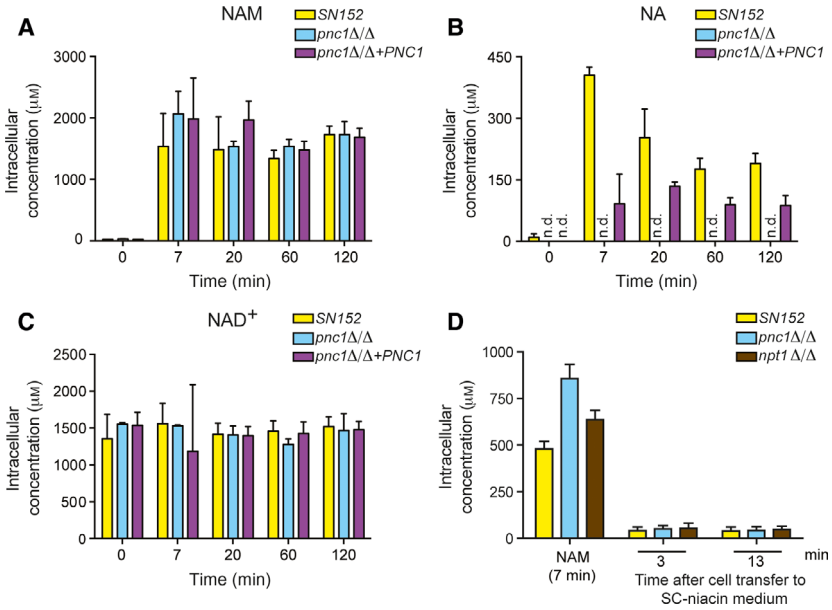

Fig. 4. *C. albicans* cells lacking the nicotinamidase Pnc1 cannot convert NAM into NA. (A-C), Cells exponentially growing in SC-Niacin medium at 30 °C were continuously exposed to 5 mM NAM for 7 min up to 120 min. Aliquots of those cells were harvested as a function of time and intracellular concentrations of NAM (A), NA (B), and NAD^+ (C) were determined by LC-MS/MS. n.d.: not detected. (D) Extensive loss of intracellular NAM following transient exposure. The three bars on the left-hand side reflect the concentrations of intracellular NAM measured after continuous exposure to 5 mM NAM for 7 min. After removing the medium containing NAM by filtration and extensive washes, the filter onto which the cells were adsorbed was transferred to SC-Niacin medium, which is devoid of NAM. Cells rapidly came off the filter, and aliquots of the cells in suspension were harvested after 3 and 13 min to determine intracellular concentrations of NAM. Panel A-C: The error bars represent the SD from the mean of three biological replicates for each strain. Panel D: The error bars represent the SD from the mean of two biological replicates for each strain.

10 min later (13-min time point in Fig. 4D). At each time point, an aliquot of cells was kept aside to determine cell numbers and cell sizes using a Coulter counter. The rest of the cells were used to determine intracellular metabolite concentrations.

Regardless of the time point at which cell suspensions were withdrawn from the SC-Niacin medium (3 or 13 min), intracellular NAM concentrations had returned to the low physiological levels (~ 25 μM NAM, Fig. 4D) typically observed in cells that were not exposed to exogenous NAM (Fig. 4A). These low concentrations of intracellular NAM were not caused by extensive cell lysis during the filtration or other steps of our procedure because cell debris were not detected using the Coulter counter, and the vast majority of cells were in the size range expected for *C. albicans*, suggesting that NAM depletion simply occurred by efflux from cells (see Discussion).

Pnc1- and Npt1-independent incorporation of NAM into NAD^+

In contrast to WT cells, mutants lacking Pnc1 cannot convert NAM into NA and, therefore, cannot incorporate NAM into NAD^+ through the canonical Preiss–Handler salvage pathway (Fig. 1, reactions **1–4**). In spite of this, NAD^+ concentrations were not significantly lower in *pnc1*Δ/Δ mutants than in WT or *PNC1* revertant cells (Fig. 4C). Based on this, we were intrigued by the possibility that *pnc1*Δ/Δ mutants might be able to generate NAD^+ from NAM through a noncanonical, Pnc1-independent mechanism. To assess whether NAM was incorporated into NAD^+ in cells lacking Pnc1, we used tetradeuterated [2,4,5,6] d_4-NAM (hereafter referred to as heavy NAM or hNAM, Fig. 5A) and quantitative metabolomics targeted to NAM- and NAD^+-related metabolites [51]. We confirmed by MS that our commercial source of d_4-NAM was essentially all tetradeuterated (data not shown). In spite of this, upon *in vivo* incorporation of NAM into NAD^+-related metabolites, we found that all our d_4-NAM was converted into di- and trideuterated NAM when incorporated into NAD^+-related nucleosides and nucleotides. There are two reasons for this. First, once d_4-NAM is incorporated into nucleosides or nucleotides, the positive charge of the N1 nitrogen renders the deuterium atom linked to C2 labile (Fig. 5A), and rapidly exchanged by a hydrogen atom derived from water [53,54]. Second, once heavy NAM is incorporated into NAD^+, the C4 position becomes active in reduction–oxidation reactions between NAD^+ and NADH, which leads to replacement of the C4-linked deuterium by hydrogen during hydride transfer reactions (Fig. 5E, red ellipse above d_4-NADH). Collectively, the loss of 1 or 2 deuterium atoms through these two processes is sufficient to account for the fact that, except for d_4-NAM itself, we did not detect NAD^+-related nucleosides or nucleotides that included d_4-NAM. Only d_2-NAM or d_3-NAM was detected in NAD^+-related nucleosides or nucleotides derived from cells treated with d_4-NAM.

In *S. cerevisiae*, NAM salvage begins with the Pnc1-mediated conversion of NAM into NA. Given this, we did not expect to find incorporation of d_4-NAM into d_2- or d_3-$hNAD^+$ in *C. albicans* *pnc1*Δ/Δ mutants where NA is undetectable (Fig. 4B). Consistent with a functional Pnc1-dependent salvage pathway, we were able to detect incorporation of hNAM into $hNAD^+$ in WT and *PNC1* revertant cells (Fig. 5D). However, incorporation of hNAM into $hNAD^+$ was unexpectedly observed in significant amounts in *pnc1*Δ/Δ and *pnc1*Δ/Δ *npt1*Δ/Δ cells, two mutants where the Preiss–Handler salvage pathway is inactivated (Fig. 5D). Because the formation of $hNAD^+$ in cells lacking Pnc1 was unanticipated, we felt it crucial to perform an experiment aimed at determining whether the deuterium atoms were truly located in the nicotinamide moiety of heavy NAD^+. Metabolite extracts from *pnc1*Δ/Δ cells exposed to light NAM or d_4-NAM were resolved by liquid chromatography (Fig. 6A,B) and the light and trideuterated forms of NAD^+ were fragmented in a mass spectrometer under conditions that broke the N-glycosidic bond between NAM and ADP-ribose. This enabled us to selectively detect the mass of the NAM moiety of NAD^+. The experimental mass was 122.0348 Da for the NAM derived from light NAD^+ (theoretical mass = 122.0480) and 125.0537 Da (theoretical mass = 125.0668) for the d_3-NAM derived from d_3-NAD^+ (Fig. 6C,D). Because the presence of small quantities of d_3-NAM in our commercially available source of d_4-NAM would have given the same results, we determined whether d_3-NAM was detectable in the commercial product by LC-MS/MS. Even with a high sensitivity instrument, we did not detect d_3-NAM (data not shown). We therefore conclude that, contrary to our initial expectations, our results demonstrate the existence of a Pnc1-independent, noncanonical mechanism for incorporation of heavy NAM into NAD^+.

We explored the possibility that the *C. albicans* nicotinic acid phosphoribosyltransferase (Fig. 1, Npt1, reaction **2**) might contribute to noncanonical incorporation of NAM into NAD^+. The rationale to suspect that this might be the case was the following. Although *S. cerevisiae* Npt1 is specific for NA [48,55], there are several precedents for enzymes that act on both the acidic and amide forms of NAD^+ precursors.

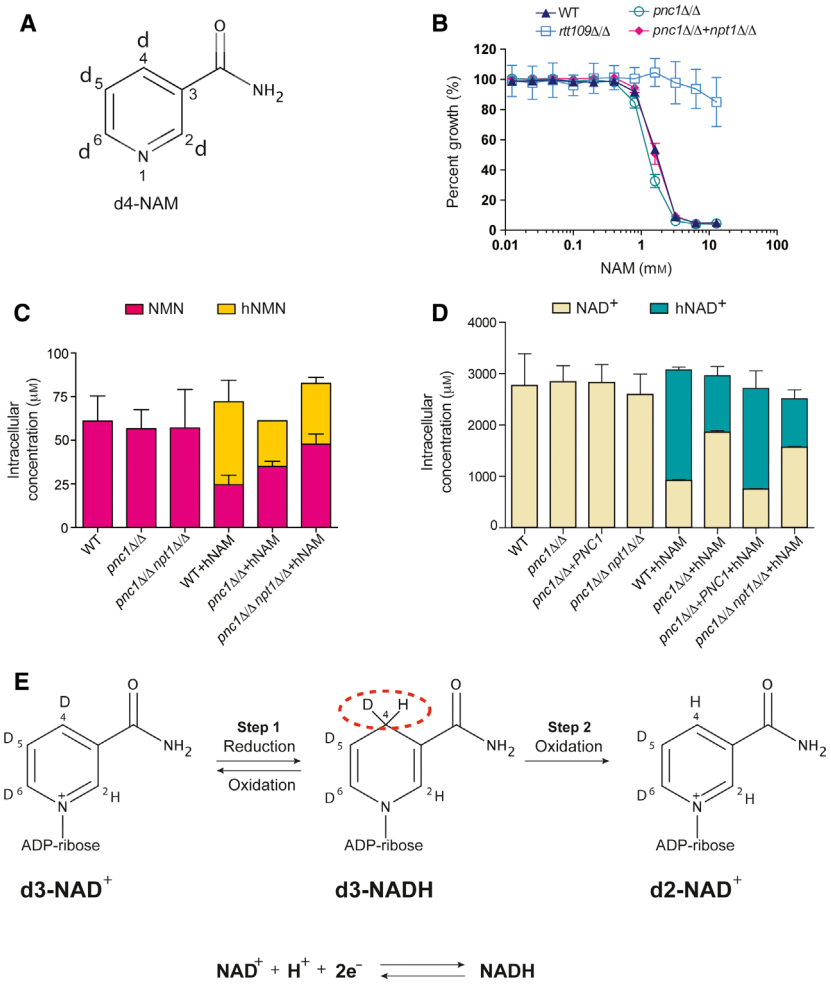

Fig. 5. Pnc1 and Npt1-independent noncanonical incorporation of hNAM into hNMN and hNAD$^+$. (A) Positions of deuterium atoms in tetradeuterated [2,4,5,6] d_4-NAM (heavy NAM or hNAM). (B) Growth inhibition assay in liquid cultures. Strains were grown at 30 °C for 24 h in SC-Niacin medium containing increasing concentrations of NAM prior to measuring the optical density at 600 nm (OD600). The percentage growth is the ratio of OD600 values in wells containing NAM over that of control wells that lack NAM. Panel B: The error bars represent the SD from the mean of either nine (WT, *rtt109*Δ/Δ, and *pnc1*Δ/Δ) or six biological replicates (*pnc1*Δ/Δ*npt1*Δ/Δdouble mutant). Please note that the means of the nine replicates for WT, *rtt109*Δ/Δ, and *pnc1*Δ/Δ cells were derived from three independent experiments, each performed as three biological replicates for Figs. 3A, 5B, and 7A (see Supplementary Tables for the raw data). As a result, the curves for WT, *rtt109*Δ/Δ, and *pnc1*Δ/Δ cells are identical in Figs. 3A, 5B, and 7A. (C-D) Cells growing in SC-Niacin were exposed to 5 mM hNAM for 2 h or left untreated. Concentrations of light and hNMN (C) or light and hNAD$^+$ (D) were determined by LC-MS/MS. Panels C-D: The error bars represent the SD from the mean of 4 biological replicates (WT, *pnc1*Δ/Δ, *pnc1*Δ/Δ*npt1*Δ/Δ double mutant, and *pnc1*Δ/Δ + *PNC1* revertant). Panel C: The hNMN (orange) in the *pnc1*Δ/Δ column is devoid of error bar because NMN concentrations were systematically low and, even though NMN was detected in all our experiments, hNMN was below our limit of quantification in three out of four experiments with this mutant. Given this, it would have been misleading to include an error bar for the abundance of hNMN in the *pnc1*Δ/Δ cells. (E) Reversible reduction of NAD$^+$ results in the loss of a deuterium atom from the C4 position of the NAM moiety of NAD$^+$. During step 1, the reduction of d_3-NAD$^+$ (labeled in positions 4, 5, and 6 of the NAM moiety) to d_3-NADH, the C4 position of the NAM moiety becomes covalently linked to both hydrogen and deuterium atoms (dotted red oval). During step 2, the oxidation of NADH that regenerates NAD$^+$, either the hydrogen or the deuterium can be released, but loss of the deuterium from the C4 position results in the formation of d_2-NAD$^+$.

This is the case, for example, of *Acinetobacter baumanii* NadM [56], a homologue of eukaryotic Npt1, and *S. cerevisiae* Nma1 and Nma2 that adenylate either nicotinic acid mononucleotide (NaMN) or nicotinamide mononucleotide (NMN) (Fig. 1, reactions **3a** and **3b**) [57–59]. This is also true of

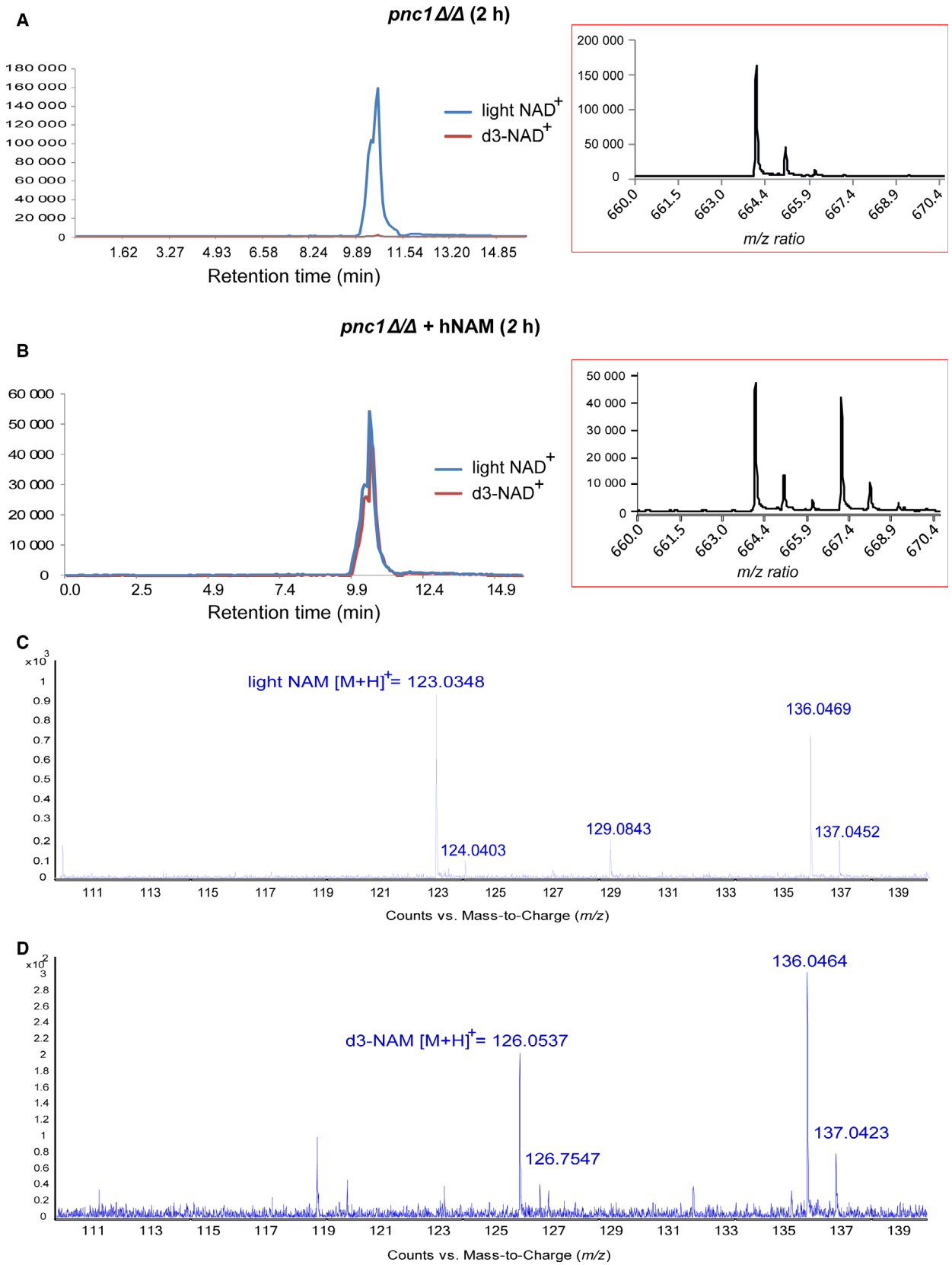
A
pnc1Δ/Δ (2 h)
light NAD+
d3-NAD+
Retention time (min)
m/z ratio
B
pnc1Δ/Δ + hNAM (2 h)
light NAD+
d3-NAD+
Retention time (min)
m/z ratio
C
light NAM [M+H]+= 123.0348
136.0469
129.0843
137.0452
124.0403
Counts vs. Mass-to-Charge (m/z)
D
136.0464
d3-NAM [M+H]+= 126.0537
137.0423
126.7547
Counts vs. Mass-to-Charge (m/z)

Fig. 6. LC-MS/MS detection of nicotinamide moieties derived from light and heavy d3-NAD^+. *pnc1*Δ/Δ cells growing in SC-Niacin were exposed to either 5 mM light NAM (A and C) or 5 mM heavy NAM (B and D) for 2 h at 30 °C, and extracted metabolites were analyzed by LC-MS/MS. (A) Retention time of light NAD^+ during RP-HPLC. Inset: [^{13}C] isotopic series of light NAD^+. (B) Retention time of light NAD^+ and d_3-NAD^+ during RP-HPLC. Inset: [^{13}C] isotopic series of both light NAD^+ and d_3-NAD^+. (C) Fragmentation spectrum of the precursor ion corresponding to light NAD^+ (shown in A). The singly protonated ion at *m/z* 123.0348 corresponds to light NAM derived from light NAD^+. (D) Fragmentation spectrum of the precursor ion corresponding to d_3-NAD^+ (shown in B). The singly protonated ion at *m/z* 126.0537 corresponds to d_3-NAM derived from d_3-NAD^+.

nicotinamide riboside kinase (Nrk1), which can phosphorylate either NR (Fig. 1, reaction **6**) or nicotinic acid riboside (NaR, not shown in Fig. 1) [60]. Given this, we asked whether, in addition to converting NA into NaMN (Fig. 1, reaction **2**), *C. albicans* Npt1 might also utilize NAM as substrate to produce NMN. To address the role of Npt1 in noncanonical synthesis of NAD^+, we deleted both alleles of the *NPT1* gene in our *pnc1*Δ/Δ null mutant strain. In the resulting *pnc1*Δ/Δ *npt1*Δ/Δ double mutant strain, the prediction is that NAM cannot be deamidated into NA because of the *pnc1*Δ/Δ mutation or converted into NMN because of the *npt1*Δ/Δ mutation. If this were true, NAM should accumulate to higher levels than in WT cells because it should not be converted into either NA or NMN in *pnc1*Δ /Δ *npt1*Δ /Δ double mutants. This did not seem to be the case because *pnc1*Δ/Δ *npt1*Δ/Δ double mutants were not more sensitive to NAM than WT cells or *pnc1*Δ/Δ single mutants (Fig. 5B, pink diamonds versus black triangles). Consistent with the fact that their sensitivity to NAM was not greater than that of WT cells, cells lacking both Pnc1 and Npt1 retained the ability to incorporate hNAM into either hNMN or $hNAD^+$. For instance, hNMN formation by the *pnc1*Δ/Δ *npt1*Δ/Δ double mutant reached ~ 75% of the amount of hNMN generated by WT cells (Fig. 5C, orange bars). Similarly, incorporation of hNAM into $hNAD^+$ in the *pnc1*Δ/Δ *npt1*Δ/Δ double mutant reached ~ 45% of the amount of $hNAD^+$ produced by WT cells (Fig. 5D, blue bars). This formally rules out the possibility that *C. albicans* Pnc1 and Npt1 are essential for incorporation of hNAM into hNMN or $hNAD^+$. This implies the existence of at least one other process that results in hNAM incorporation into hNMN and $hNAD^+$.

Noncanonical incorporation of NAM into NMN and NAD^+ does not proceed through formation of NR

In *S. cerevisiae*, NR can be salvaged to generate NAD^+ via two distinct routes. First, NR can be phosphorylated by Nrk1 to generate NMN (Fig. 1, reaction **6**), followed by adenylation of NMN to produce NAD^+ (Fig. 1, reaction **3b**) [48]. Second, the NAM moiety of NR can be cleaved from the ribose (Fig. 1, reaction **5**), and the resulting NAM can enter the Pnc1-dependent canonical NAM salvage pathway [61]. In *S. cerevisiae*, production of NAM from NR can be catalyzed by three enzymes: the phosphorylase Pnp1, the nucleosidase Urh1, and, to a much lesser extent, the phosphorylase Meu1 (Fig. 1, reaction **5**) [61]. The reactions catalyzed by nucleosidases and phosphorylases are generally considered irreversible. However, given the supraphysiological concentrations of NAM employed in some of our experiments, we could not exclude the possibility that some hNAM might be converted into hNR through reversal of reaction **5** (Fig. 1). If this were the case, the aforementioned Nrk1-mediated phosphorylation of NR would salvage hNR by converting it into hNMN (Fig. 1, reaction **6**), and subsequent adenylation of hNMN would generate $hNAD^+$ (Fig. 1, reaction **3b**).

In order to test whether hNAM can be converted into hNR, we initially attempted to disrupt the *PNP1* and *URH1* genes using clustered regularly interspaced short palindromic repeats (CRISPR)/Cas9-mediated gene targeting but, despite numerous attempts with different guide RNAs, this strategy failed. As an alternative strategy, we reasoned that if reaction **5** (Fig. 1) were reversible at supraphysiological concentrations of hNAM, disruption of the *NRK1* gene should result in an accumulation of hNR because it would be trapped between reactions **5** and **6** in the absence of Nrk1 (Fig. 1). To address this possibility, we exploited CRISPR/Cas9-mediated gene targeting adapted to *C. albicans* [62] to introduce premature stop codons within both alleles of the *NRK1* gene in *pnc1*Δ/Δ cells. Cells lacking both Pnc1 and Nrk1 were, at best, slightly more sensitive to NAM than *pnc1*Δ/Δ single mutants or WT cells (Fig. 7A, green circles). Even if reversal of reaction **5** (Fig. 1) were possible at supraphysiological NAM concentrations, the absence of Nrk1 should prevent incorporation of hNR into either hNMN or $hNAD^+$ via the Nrk1 branch of the NR salvage pathway (Fig. 1). This was clearly not the case. Upon exposure to 5 mM hNAM, both hNMN and $hNAD^+$ were produced by *pnc1*Δ/Δ *nrk1*$^{CR/CR}$ double

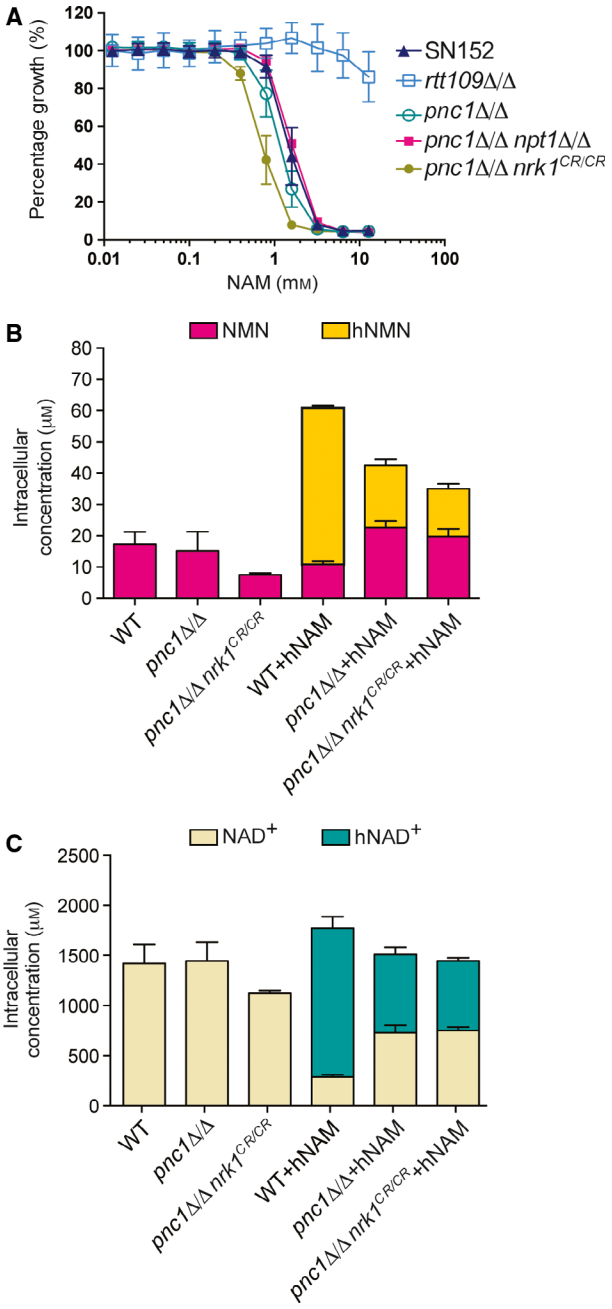

Fig. 7. Nrk1 and Pnc1 are dispensable for incorporation of hNAM into hNMN and hNAD$^+$. (A) Growth inhibition assay in liquid cultures. Strains were grown at 30 °C for 24 h in SC-Niacin medium containing increasing concentrations of NAM prior to measuring the optical density at 595 nm (OD595). The percentage growth is the ratio of OD595 values in wells containing NAM over the OD595 values of control wells lacking NAM. Panel 7A: The error bars represent the SD from the mean of either nine (WT, *rtt109*Δ/Δ, and *pnc1*Δ/Δ) or six biological replicates (*pnc1*Δ/Δ*npt1*Δ/Δ and *pnc1*Δ/Δ*nrk1*$^{CR/CR}$ double mutants). Please note that the means of the nine replicates for WT, *rtt109*Δ/Δ, and *pnc1*Δ/Δ cells were derived from three independent experiments, each performed as three biological replicates for Figs. 3A, 5B, and 7A (see Supplementary Tables for the raw data). As a result, the curves for WT, *rtt109*Δ/Δ, and *pnc1*Δ/Δ cells are identical in Figs. 3A, 5B, and 7A. (B-C) Cells growing in SC-Niacin were exposed to 5 mM hNAM for 2 h or left untreated. Concentrations of light and hNMN (B) or light and hNAD$^+$ (C) were determined by LC-MS/MS. Panels 7B-C: The error bars represent the SD from the mean of three biological replicates for each strain.

mutant cells (Fig. 7B,C). In addition, even when *pnc1*Δ/Δ *nrk1*$^{CR/CR}$ mutants were exposed to 5 mM hNAM for 2 h, the hNR concentrations that we detected following a 2-h exposure to 5 mM hNAM were either below the limit of quantification in some experiments or barely above it in other experiments (data not shown). Hence, the double mutant *pnc1*Δ/Δ *nrk1*$^{CR/CR}$ did not accumulate high concentrations of hNR. These two results argue against the possibility that high concentrations of hNAM might drive its conversion into hNR through the chemically improbable reversal of reaction **5** (Fig. 1). We noticed that the ratio of hNMN over endogenous light NMN was ~ 5.0-fold higher *pnc1*Δ/Δ single mutants (Fig. 7B, orange bars over pink bars). Similarly, the ratios of hNAD$^+$ over light NAD$^+$ were ~ 5.2-fold higher in WT cells than in our *pnc1*Δ/Δ single mutant (Fig. 7C, blue bars over beige bars). These results demonstrate that, in comparison with endogenous light NAD$^+$, a greater portion of heavy NAM is incorporated into hNMN and hNAD$^+$ in WT cells than in cells lacking Pnc1. This indicates that, in WT cells fed with hNAM, biogenesis of hNAD$^+$ predominantly occurs through the Pnc1-fueled Preiss–Handler salvage pathway. Nonetheless, considerable amounts of hNAM are incorporated into hNMN and hNAD$^+$ through a non-canonical Pnc1-independent mechanism.

Noncanonical incorporation of NAM into NAD$^+$ cannot sustain cell proliferation

In WT *C. albicans* grown in SC-Niacin, we measured NAM concentrations that varied between 25 and 75 μM by LC-MS/MS. Following a 2-h continuous exposure to 100 μM d_4-NAM (a concentration that is only slightly higher than the physiological NAM concentrations that we measured in SC-Niacin), we detected incorporation of hNAM into hNAD$^+$ and hNMN in WT cells (Fig. 8A,B, WT + d_4-NAM). Even at this relatively low concentration of d_4-NAM (100 μM), hNAD$^+$ and hNMN were also generated in *pnc1*Δ/Δ cells, but at substantially lower levels than in

WT cells (Fig. 8A,B, *pnc1*Δ/Δ + d_4-NAM versus WT + d_4-NAM). This is expected because the canonical NAM salvage pathway, which is the predominant source of $hNAD^+$ in WT cells, but disabled in cells lacking Pnc1. However, the result obtained in *pnc1*Δ/Δ cells demonstrates that the noncanonical incorporation of hNAM into $hNAD^+$ does occur even when cells are exposed to a near physiological NAM concentration (100 μM).

This prompted us to design a strategy to determine whether noncanonical incorporation of NAM into NAD^+ was sufficient to allow cell proliferation in mutants that cannot synthesize NAD^+ from tryptophan (Trp) or the salvageable precursors NAM and NA. To address this possibility, we needed a system with which we could simultaneously inactivate both *de novo* synthesis of NAD^+ from Trp and canonical NAM salvage through the Preiss–Handler pathway. For this purpose, we employed a Gene Replacement and Conditional Expression strain (GRACE) that enables conditional depletion of NAD^+ synthetase (Qns1) using doxycycline (Dox). In the original strain, which we termed $qns1^{G/\Delta}$, one allele of the *QNS1* gene is deleted, whereas the remaining allele is under the control of a Dox-repressible promoter (*qns1*Δ/*pTET-QNS1*). In the absence of Qns1 (Fig. 1, reaction **4**), neither *de novo* synthesis from Trp nor canonical NAM salvage can serve as sources of NAD^+ (Fig. 1). The $qns1^{G/\Delta}$ strain exposed to Dox therefore cannot proliferate in SC-Niacin medium (which lacks NAM, NA, and NR) unless it is supplemented with NR [48], which can be salvaged by Nrk1 to generate NAD^+ even in the absence of Qns1 (Fig. 1, reactions **6** and **3b**). To deplete the Qns1 enzyme as extensively as possible, we grew cells overnight in SC-Niacin containing Dox, and 10 μM NR to preserve cell viability. As a control to ensure that Qns1 had been sufficiently depleted to cripple synthesis of NAD^+ and impair proliferation, we transferred $qns1^{G/\Delta}$ cells to SC-Niacin medium containing Dox, but lacking the three salvageable NAD^+ precursors (NAM, NA, and NR). Under those conditions, $qns1^{G/\Delta}$ cells did not proliferate (Fig. 8D, $qns1^{G/\Delta}$ + Dox). As judged by monitoring the optical density every 15 min, $qns1^{G/\Delta}$ cells exposed to Dox proliferated when SC-Niacin was supplemented with 200 μM NR as a source of NAD^+ (Fig. 8D, $qns1^{G/\Delta}$ + Dox + NR), but proliferation was abolished in SC-Niacin containing Dox and 100 μM NAM, rather than NR (Fig. 8D, strain $qns1^{G/\Delta}$ + Dox + NAM). Our results indicate that, due to depletion of Qns1, $qns1^{G/\Delta}$ cells exposed to Dox could not generate enough NAD^+ from either Trp or the canonical NAM salvage pathway. This result suggests that, in the presence of 100 μM NAM, noncanonical incorporation of NAM into NAD^+ is insufficient to support cell proliferation.

In $qns1^{G/\Delta}$ cells exposed to Dox, the canonical salvage pathway is blocked just prior to NAD^+ synthesis due to Qns1 depletion (Fig. 1, reaction **4**). However, all the earlier steps of the NAM salvage pathway (Fig. 1, reactions **1**, **2**, **3a**) are intact. Given this, Pnc1-mediated conversion of NAM into NA in Qns1-depleted cells would effectively channel NAM into a cul-de-sac (Fig. 1, reactions **2** and **3a**) containing NAM-derived salvage pathway metabolites (NA, NaMN, NaAD) that, ultimately, cannot produce NAD^+ due to the depletion of Qns1. Because Pnc1 is the first enzyme involved in canonical NAM salvage, the absence of Pnc1 should preclude this futile conversion of limiting amounts of NAM into NA, NaMN, or NaAD (Fig. 1, reactions **1**, **2,** and **3a**) and thereby increase the amount of NAM available for noncanonical synthesis of NAD^+. In order to test this hypothesis, $qns1^{G/\Delta}$ cells were genetically modified using CRISPR/Cas9-mediated insertion of premature stop codons within the two *PNC1* alleles (Materials and methods). The resulting strain was termed $qns1^{G/\Delta}$ $pnc1^{CR/CR}$. As a control, we confirmed that, even at very high NAM concentrations (> 3 mM), this strain was incapable of converting NAM into NA because of *PNC1* loss of function (Fig. 8C), thus validating that CRISPR/Cas9-mediated inactivation of both *PNC1* alleles was correct.

Following overnight depletion of Qns1 in the presence of Dox and NR (to preserve cell viability), our $qns1^{G/\Delta}$ $pnc1^{CR/CR}$ mutant strain thrived in SC-Niacin medium containing Dox and 100 μM NR (Fig. 8D, $qns1^{G/\Delta}$ $pnc1^{CR/CR}$ + Dox + NR), but failed to proliferate in the presence of Dox and 100 μM NAM (Fig. 8D, $qns1^{G/\Delta}$ $pnc1^{CR/CR}$ + Dox + NAM). This demonstrates that, even in the presence of 100 μM NAM that cannot be diverted into a nonproductive salvage pathway, noncanonical incorporation of NAM into NAD^+ cannot produce enough NAD^+ to sustain *C. albicans* proliferation. In fact, we found that over a range from physiological (50 μM) to supraphysiological (800 μM) concentrations, NAM was ineffective to rescue proliferation when Qns1 was depleted from WT (Fig. 8E, cyan bars) or Pnc1-deficient cells (Fig. 8F, cyan bars). This is in striking contrast to NR, which can rescue the lethality of *C. albicans* cells lacking both Qns1 and Pnc1 when present at a concentration as low as 50 μM NR (Fig. 8E,F, yellow bars). Our attempts to perform this experiment at NAM concentrations higher than 800 μM were thwarted by the fact that NAM inhibits Hst3, which in turn causes extensive DNA damage and cripples proliferation even when the cells are capable of synthesizing sufficient

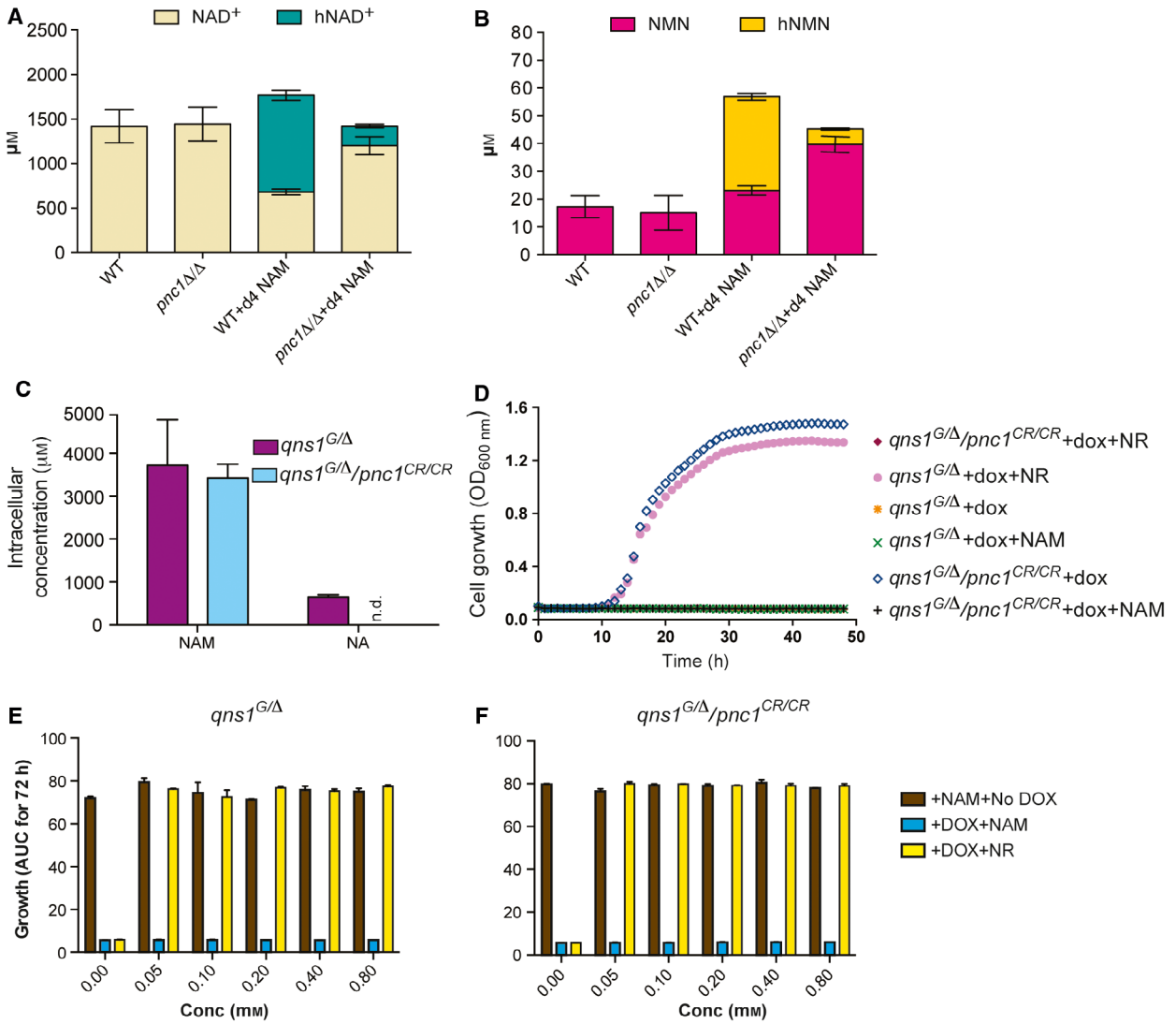

amounts of NAD^+ to maintain viability. Taken together, our results indicate that the noncanonical incorporation of NAM into NAD^+ that we uncovered cannot produce enough NAD^+ to sustain cell proliferation when both the *de novo* synthesis of NAD^+ from Trp and the NAM salvage pathway are disabled in the same cells by Qns1 depletion and *PNC1* loss of function (Fig. 8D).

Noncanonical incorporation of NAM into NAD^+ is partially inhibited by isonicotinamide

Unlike deacetylases that simply hydrolyze acetyl groups from their substrates, sirtuins require NAD^+ as an obligate substrate to deacetylate proteins [30,63–65]. During the first step of the reaction, the NAM moiety of NAD^+ is cleaved off, and the ADP-ribose portion of NAD^+ becomes covalently linked to the acetyl group of the peptide substrate to generate an O-alkylimidate reaction intermediate (Fig. 9A) [66–68]. The O-alkylimidate intermediate can then generate the deacetylated peptide, O-acetyl-ADP-ribose, and NAM (Fig. 9A) [66–68]. Alternatively, the O-alkylimidate can be intercepted by a NAM molecule, which regenerates NAD^+ and the acetylated substrate (Fig. 9B), and effectively inhibits sirtuin-mediated deacetylation [30,31,69]. Strictly speaking, the terms NAM exchange or base exchange that are often used to describe this reaction refer to the two-step reaction: cleavage of the NAM moiety derived from the starting NAD^+ molecule (light NAM, middle of Fig. 9A) followed by NAM replacement with a different NAM molecule

Fig. 8. Noncanonical incorporation of NAM into NAD^+ is insufficient to sustain *C. albicans* proliferation. (A-B) Cells growing in SC-Niacin were exposed to 100 μM hNAM for 2 h at 30 °C, and metabolite concentrations were determined by LC-MS/MS. Panel (A) shows the levels of light NAD^+ and $hNAD^+$, whereas panel (B) shows the concentrations of light NMN and hNMN. The error bars represent the SD from the mean of three biological replicates for each strain. (C) *QNS1* was repressed with Dox in cells expressing Pnc1 (*qns1*$^{G/\Delta}$ strain) or cells with CRISPR/Cas9-generated premature stop codons in both *PNC1* alleles (*qns1*$^{G/\Delta}$ *pnc1*$^{CR/CR}$ strain). Following overnight repression of the *QNS1* promoter with Dox in medium containing 10 μM NR to preserve cell viability, 5 mM NAM was added for 2 h and the levels of NAM and NA determined by LC-MS/MS. n.d.: NA was below the detection threshold in the *qns1*$^{G/\Delta}$ *pnc1*$^{CR/CR}$ strain. Panel C: The error bars represent the SD from the mean of two or four biological replicates, respectively, for the *qns1*$^{G/\Delta}$ and the *qns1*$^{G/\Delta}$ *pnc1*$^{CR/CR}$ strains. (D) Dox-induced repression of *QNS1* was conducted overnight in medium containing 10 μM NR to preserve cell viability. Cultures were diluted to OD600 = 0.0005 in SC-Niacin + Dox and either 100 μM NR or 100 μM NAM. Cell growth was monitored every 15 min up to 48 h. Only the two strains grown in media containing NR (*qns1*$^{G/\Delta}$ + dox + NR, pink circles, and *qns1*$^{G/\Delta}$ *pnc1*$^{CR/CR}$ + dox + NR, blue diamonds) showed robust growth under these conditions. All the other strains failed to grow: The flat horizontal line contains data from four conditions: *qns1*$^{G/\Delta}$ + dox; *qns1*$^{G/\Delta}$ + dox + NAM; *qns1*$^{G/\Delta}$ *pnc1*$^{CR/CR}$ + dox; and *qns1*$^{G/\Delta}$ *pnc1*$^{CR/CR}$ + dox + NAM). Two biological replicates were conducted with each strain. (E-F) Strains where the only allele of the *QNS1* gene was repressible with Dox (*qns1*$^{G/\Delta}$) were incubated overnight in SC-Niacin containing Dox and 10 μM NR to deplete Qns1 while preserving viability with NR. Strains *qns1*$^{G/\Delta}$ (E) and *qns1*$^{G/\Delta}$ *pnc1*$^{CR/CR}$ (F) were grown in SC-Niacin supplemented with increasing concentrations of either NR or NAM, and in the absence or presence of Dox to repress *QNS1*. Growth was monitored by measuring the optical density at 600 nm every 15 min for up to 72 h. As described in the Materials and methods, growth curves were transformed into numerical values (arbitrary units) that are proportional to the areas under the growth curves (AUC). Panels E-F: The *x*-axes are labeled 'Concentration (mM)' for simplicity but, as implied from the key to the color codes on the right of panel F, for the brown and blue bars the *x*-axes represent NAM concentrations. In contrast, the *x*-axes represent NR concentrations for the yellow bars. The error bars represent the SD from the mean of two biological replicates for each condition.

(hNAM or d_4-NAM, Fig. 9B). However, for simplicity, we adopted the convention that the NAM exchange reaction only refers to the reverse reaction illustrated in Fig. 9B.

Isonicotinamide (isoNAM) is an isostere of NAM in which the carboxamide group is linked to C4 of the pyridine ring, rather than C3 in the case of NAM (Fig. 9C). Because of their similarity, isoNAM weakly competes with NAM and prevents it from reacting with the O-alkylimidate intermediate. As a result, isoNAM inhibits the NAM exchange reaction (defined as shown in Fig. 9B) and, consequently, isoNAM enhances the deacetylase activity of sirtuins [70]. Consistent with its ability to enhance sirtuin activity, high concentrations of isoNAM (> 25 mM) have been employed in *S. cerevisiae* to increase the repression of genes whose silencing requires Sir2-dependent histone deacetylation [70,71]. *In vitro*, isoNAM is a weak inhibitor of the NAM exchange reaction (Ki = 68 mM). Nonetheless, isoNAM did enhance *S. cerevisiae* Sir2-mediated deacetylation of histone H4-derived peptides *in vitro* [70]. In spite of its weak inhibition of the NAM exchange reaction, we sought to take advantage of isoNAM to determine whether noncanonical incorporation of hNAM into $hNAD^+$ might occur through the NAM exchange reaction *in vivo*. For these experiments, we used *pnc1*Δ/Δ cells in which canonical NAM salvage is blocked, thereby enabling us to selectively study the noncanonical incorporation of NAM into NAD^+. Cells lacking Pnc1 were exposed to 0.2 mM hNAM for 2 h in the presence of concentrations of isoNAM ranging from 0 to 80 mM. At high isoNAM concentrations (40 or 80 mM), we observed a decrease in the levels of light NAD^+ that culminated in an ~ 2-fold decrease in light NAD^+ at 80 mM isoNAM (Fig. 9D). This decrease in the abundance of light NAD^+ may, at least in part, be caused by the ability of isoNAM to increase the deacetylase activity of sirtuins, a reaction that consumes NAD^+. The decrease in the concentration of $hNAD^+$ was ~ 4-fold at 80 mM isoNAM (Fig. 9E). Hence, high concentrations of isoNAM impaired, but did not completely abolish the incorporation of hNAM into $hNAD^+$. This result suggests that the noncanonical incorporation of hNAM into $hNAD^+$ is, at least in part, mediated through a sirtuin-dependent NAM exchange reaction that is partially inhibited by high concentrations of isoNAM. Because 80 mM isoNAM only partially inhibited the incorporation of hNAM into $hNAD^+$, we cannot formally exclude the possibility that noncanonical mechanisms other than the NAM exchange reaction may contribute to the formation of $hNAD^+$. However, it is equally plausible that the incomplete inhibition merely reflects the fact that isoNAM is a very weak inhibitor of the NAM exchange reaction. Unfortunately, isoNAM is the only known inhibitor of the NAM exchange reaction. In an effort to obtain a more complete inhibition of the NAM exchange reaction, we tested another isostere of NAM known as 2-pyridine carboxamide (picolinamide), side-by-side with isoNAM. Unfortunately, even at 80 mM, picolinamide proved incapable of inhibiting the incorporation of hNAM into $hNAD^+$.

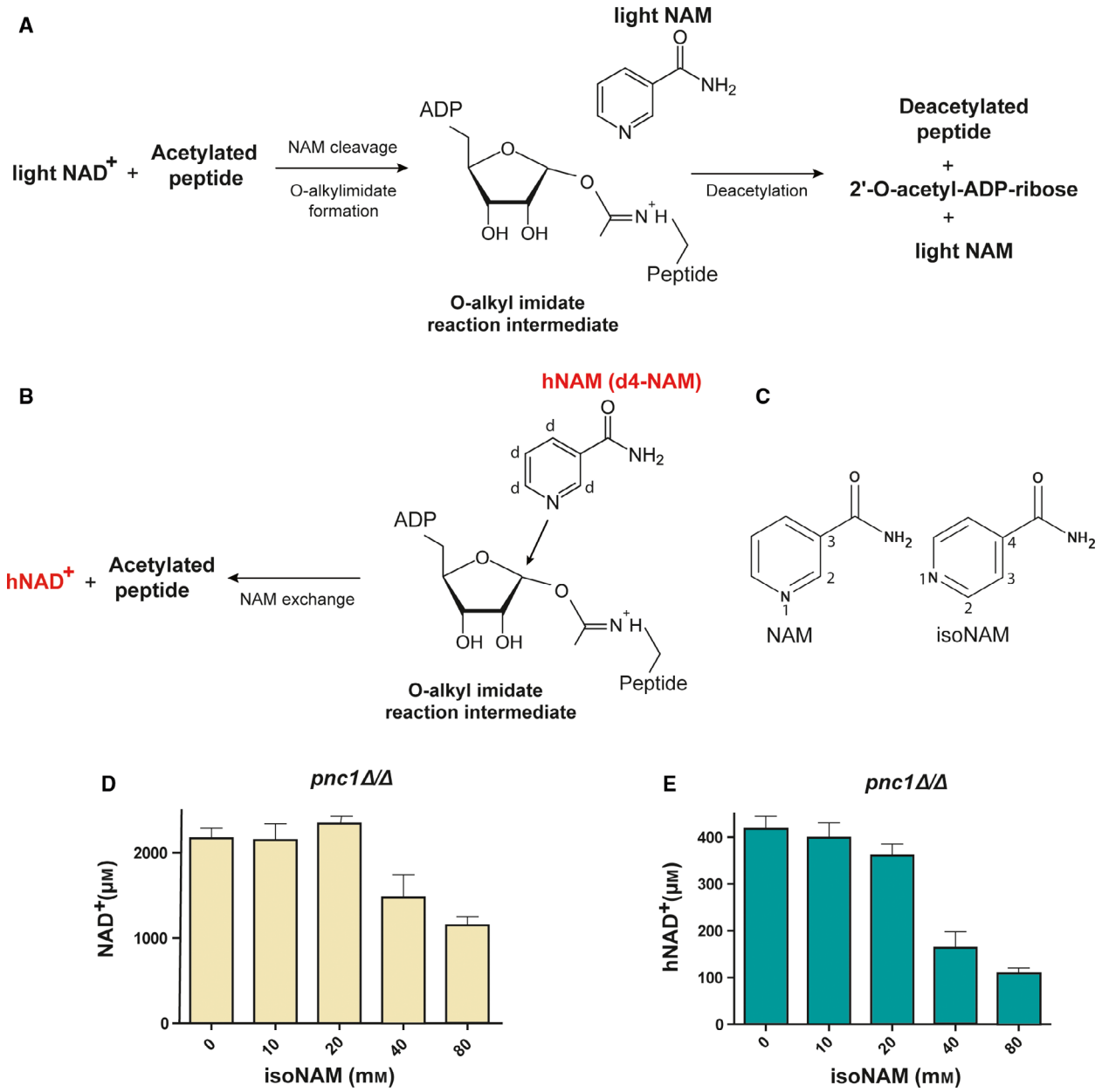

Fig. 9. Noncanonical incorporation of NAM into NAD^+ is partially inhibited by isoNAM. (A) NAD^+-dependent protein deacetylation by sirtuins: The figure emphasizes the early departure of light NAM cleaved from NAD^+. The figure also shows the O-alkylimidate reaction intermediate in which the ADP-ribose portion of NAD^+ is covalently linked to the acetyl group of the target lysine in the peptide or protein substrate. (B) The NAM exchange reaction results in inhibition of sirtuin-mediated protein deacetylation. The diagram highlights the fact that, in our experiments, the NAM exchange reaction is initiated by a heavy molecule of NAM, and culminates in formation of heavy NAD^+. (C) Chemical structures of NAM and isoNAM, an inhibitor of the NAM exchange reaction. (D-E) *pnc1*Δ/Δ cells growing in SC-Niacin were exposed to 0.2 mM hNAM and increasing concentrations of isoNAM for 2 h. The concentrations of light NAD^+ (D) and heavy NAD^+ (E) were determined by LC-MS/MS. Panels D-E: The error bars represent the SD from the mean of three biological replicates.

Discussion

We previously reported that the cytotoxicity of supraphysiological NAM concentrations (~ 1–2 mM NAM) in *C. albicans* was exerted through inhibition of the sirtuin Hst3 [11]. In an effort to enhance the cytotoxicity of NAM toward *C. albicans* and other fungal pathogens, we set out herein to uncover the fates of

supraphysiological concentrations of NAM. We demonstrated that NAM had three distinct fates. The first is the Pnc1-dependent conversion of NAM into NA (Fig. 1, reaction **1**), which serves as a prelude to the Preiss–Handler salvage pathway that ultimately generates NAD^+. The second fate of NAM was uncovered in experiments where cells were transiently exposed to supraphysiological NAM concentrations. Under these conditions, a striking efflux of NAM led to restoration of physiological intracellular concentrations (25–75 μM). Thirdly, we showed that NAM enters a futile cycle through the so-called NAM or base exchange reaction that occurs when a NAM molecule intercepts the O-alkylimidate reaction intermediate produced during the deacetylation of sirtuin substrates (Fig. 9A,B). The NAM exchange reaction does not result in consumption of NAM molecules (Fig. 9A,B) and, therefore, cannot augment the resistance to NAM of *C. albicans* or other fungal pathogens.

Noncanonical incorporation of NAM into NAD^+ and NMN

We provided evidence for the existence of a noncanonical (Pnc1-independent) mechanism through which heavy NAM (hNAM) was incorporated into $hNAD^+$ and hNMN even at near physiological NAM concentration (100 μM, Fig. 8A,B). This noncanonical mechanism likely involves, at least in part, the incorporation of NAM into NAD^+ through a sirtuin-dependent NAM exchange reaction, also known as base exchange reaction, that is partially inhibited by isoNAM (Fig. 9E). During sirtuin-mediated deacetylation, cleavage of the NAM moiety of NAD^+ is prerequisite for the formation of the O-alkylimidate reaction intermediate (Fig. 9A). Because of this, another NAM molecule (e.g., d4-NAM, as illustrated in Fig. 9B) can only initiate the NAM exchange reaction after cleavage of NAM from the original NAD^+ substrate and formation of the O-alkylimidate reaction intermediate (Fig. 9A). The net result of NAD^+ cleavage and release of its NAM moiety (Fig. 9A), followed by NAM consumption to regenerate NAD^+ (Fig. 9B), constitutes a two-step futile cycle that does not consume NAM molecules and, therefore, cannot contribute to NAM resistance.

In contrast to the NAM exchange reaction by which NAM incorporation directly generates NAD^+, there is no known fungal enzyme or mechanism by which NMN would be produced by direct incorporation of NAM. In contrast to fungi, direct conversion of NAM into NMN is catalyzed by NAM phosphoribosyltransferase (NAMPT) in metazoans [37]. The closest homologue of NAMPT in *C. albicans* is the Npt1. *S. cerevisiae* Npt1 is strictly specific for NA, and cannot employ NAM as a substrate. Consistent with the specificity of *S. cerevisiae* Npt1 for NA, we found that, even when exposed to high concentrations of NAM (5 mM), *C. albicans pnc1 npt1* double mutants were as proficient as *pnc1* single mutants in converting hNAM into hNMN (Fig. 5C). This shows that *C. albicans* Npt1 is not essential for generation of NMN from NAM, even when NAM is present at supraphysiological concentrations. However, we cannot formally rule out the possibility that *C. albicans* Npt1 may act in a redundant manner with an unknown enzyme(s) to promote the biosynthesis of NMN from NAM.

Since no ribosyltransferase other than Npt1 is known to act on molecules chemically similar to NAM, we propose the following pathway to explain the noncanonical incorporation of NAM into NMN. The first step is the incorporation of hNAM into $hNAD^+$ via the sirtuin-dependent NAM exchange reaction. Second, $hNAD^+$ could be deadenylated through reversal of the reaction catalyzed by Nma1 (Fig. 1, reverse of reaction **3b**), thereby resulting in the formation of hNMN. *In vitro,* adenylation of NMN to produce NAD^+ is readily reversible [72]. Adenylation of NMN requires ATP and generates NAD^+ together with inorganic pyrophosphate (PPi) (Fig. 1, inset). In order to drive the reversible adenylation–deadenylation reaction catalyzed by Nma1 toward biogenesis of NAD^+ *in vivo*, the PPi produced by adenylation of NMN is hydrolyzed by inorganic pyrophosphatase (Ipp1, Fig. 1 inset) [73]. Because the hydrolysis of PPi is strongly exergonic, the sequential activities of Nma1 and Ipp1 (Fig. 1 inset) greatly favor adenylation of NMN to generate NAD^+ [73]. *C. albicans* possesses a constitutively expressed inorganic pyrophosphatase known as Ipp1 [74,75]. In spite of this, we feel that even a modest degree of reversibility may be sufficient to account for conversion of $hNAD^+$ into hNMN. This is because the concentration of NAD^+ in cells lacking Pnc1 (up to 3000 μM in Fig. 5D) is considerably higher than that of NMN (between 50 and 75 μM in Fig. 5C), which would favor some degree of deadenylation of NAD^+.

NAM efflux

Three lines of evidence argue that conversion of NAM into other metabolites is not the main mechanism by which the intracellular concentration of NAM dramatically decreases in transient exposure experiments.

First, even though Pnc1 is the only enzyme that converts NAM into NA in *C. albicans* (Fig. 4B), the residual intracellular NAM concentrations following removal of NAM from the medium were not significantly higher in *pnc1* mutants than in WT cells (Fig. 4D). Second, if the majority of NAM molecules were depleted by Pnc1-dependent conversion of NAM into NA in WT cells, one would expect a large increase in the abundance of intracellular NA in *npt1* null mutant cells because the NA would be trapped between reactions **1** and **2** (Fig. 1). However, after NAM removal from the medium, the intracellular concentration of NA did not substantially differ in WT and *npt1* null mutant cells (Fig. 4D). Third, when WT cells were transiently exposed to NAM, we did not detect intracellular accumulation of any metabolite whose biosynthesis begins with NAM (NA, NaMN, NaAD, NAD^+ or $NADP^+$). Collectively, these observations strongly suggest that the striking disappearance of intracellular NAM was not due to its conversion into NA or other metabolites that are part of the Preiss–Handler pathway. We favor the view that, when cells containing supraphysiological concentrations of NAM are transferred to SC-Niacin medium, there is an efflux of NAM molecules that restores NAM levels to their low physiological concentrations (~ 25–75 μM in SC-Niacin medium).

Because NAM molecules are small and devoid of charge, NAM likely diffuses freely across fungal cell walls and cell membranes [76,77]. Hence, NAM efflux may occur mostly, and perhaps exclusively by passive diffusion. An alternative mechanism that is not mutually exclusive with passive diffusion is the efflux of NAM by 'ATP-independent' facilitated diffusion through a membrane permease of the major facilitator superfamily (MFS) [78]. Some members of the vast repertoire of MFS transporters expressed in *C. albicans* are able to transport a number of chemically distinct entities (e.g., multidrug efflux transporters) [78]. The relaxed specificity of some MFS transporters may permit efflux of NAM when present at high concentrations.

Bioavailability of intracellular NAM for inhibition of Hst3

In vitro, the reported IC50 and Ki values for NAM-mediated inhibition of several sirtuins range (depending on each specific sirtuin, and the assays used to measure inhibition) from 33 μM NAM for inhibition of human SIRT2 and 480 μM NAM for *Thermatoga maritima* Sir2 [30,31,69,79]. Given these values, the high intracellular NAM concentrations achieved in our experiments (~ 1.5–3.5 mM NAM, Figs 4A and 8C) almost certainly inhibit, at least to some degree, all the *C. albicans* sirtuins. This is definitely the case for the sirtuin Hst3, which is the pharmacologically relevant target of NAM. Based on immunoblotting, 1–2 mM NAM clearly inhibits Hst3-mediated deacetylation of H3K56 (Fig. 3D) [11]. Unlike NAM, NA or other intermediates of the Preiss–Handler salvage pathway cannot inhibit sirtuins. Our results indicate that WT cells channel a considerable portion of the supplied NAM through the Preiss–Handler salvage pathway, thus leaving only a modest portion of NAM bioavailable to inhibit Hst3 and other sirtuins through the NAM exchange reaction. This may not be important to confer resistance to NAM under our laboratory conditions where cells are continuously exposed to high NAM concentrations. However, in a clinical setting, the substantial portion of NAM molecules converted by the pathogen into NA and other metabolites that cannot inhibit Hst3 would exacerbate the problem caused by bloodstream NAM concentrations that, according to most pharmacokinetic studies [35,36,38–40], rarely ever reach the concentrations needed for effective inhibition of Hst3.

Implications for the therapeutic potential of NAM as an antifungal agent

Although NAM conversion into NA and the efflux of NAM constitute significant obstacles to the therapeutic use of NAM, these limitations may not prove insurmountable. First, although there are large differences between the published pharmacokinetic profiles of NAM, two studies in humans reported long-lasting (median half-life of 9.3 h) and elevated circulating concentrations of NAM (0.8–2.3 mM) that are cytocidal to *C. albicans in vitro* [11]. Second, NAM has previously been shown to exert either additive or synergistic effects when combined with a number of drugs commonly employed to treat infections caused by several species of *Leishmania* parasites [80]. Pairs of drugs that function through different mechanisms often act in a synergistic, rather than additive manner [81]. Moreover, drug combination therapy often reduces the emergence of drug resistance [81]. This may prove invaluable to treat fungal infections caused by species such as *C. auris,* which have a high propensity to become multidrug-resistant [82]. Based on these considerations, it may be worth exploring the possibility of combining NAM with currently employed antifungal agents such as azoles or echinocandins. Third, with the caveat that the number of microbial cells in the

human body is rather difficult to determine accurately, and subject to reassessment over time [83], the intestinal microbiota has been reported to comprise ~ 100 trillion microorganisms, which include numerous bacterial and fungal species [84]. Based on amino acid sequence similarity, a large proportion of those bacterial and fungal species express nicotinamidases similar to Pnc1. Because Pnc1 converts NAM into NA, which cannot inhibit Hst3, the intestinal microbiota is potentially capable of consuming a significant portion of the NAM administered orally to treat systemic fungal infections. If this hypothesis is true, it may be possible to enhance the concentration of NAM in circulation and, therefore, its therapeutic potential, by transiently curtailing the intestinal microbiota using, for instance, a broad-spectrum antibiotic [85,86]. In conclusion, although the results presented in this manuscript challenge the notion that NAM may prove valuable to treat fungal infections, there remain a number of potentially valuable strategies to augment the therapeutic efficacy of NAM.

Materials and methods

Proliferation assays in liquid cultures

Minimal inhibitory concentrations were determined in liquid cultures performed as described previously in flat-bottomed 96-well plates [87]. Cells were grown overnight in SC-Niacin medium at 30 °C followed by dilution to OD_{600} = 0.0005 in 100 µL SC-Niacin medium containing 2-fold serial dilutions of a stock solution of the chemical of interest. The highest concentration for nicotinamide was 12.8 mM and 0.15% v/v for MMS. At least three independent experiments, each in duplicate, were performed. Data were plotted as percent cell growth in wells containing increasing concentrations of the chemical relative to control wells containing culture medium only. Average percent growth and standard deviations were plotted using PRISM 6 (Prism GraphPad software, San Diego, CA, USA).

To assess whether the severe growth defect of Dox-treated *qns1*$^{G/\Delta}$ and *qns1*$^{G/\Delta}$*pnc1*Δ/Δ mutant cells was rescued by nicotinamide (NAM), strain CaST207 was grown overnight at 30 °C in SC-Niacin medium supplemented with 10 µM NR and 50 µg·mL^{-1} Dox to deplete the Qns1 protein. On the next day, the cells were diluted to OD_{600} = 0.0005 in 100 µL SC-Niacin medium in a microtiter plate containing increasing concentrations of NAM or NR (from 50 µM up to 800 µM) either in the absence or presence of 50 µg·mL^{-1} Dox. The growth of cell populations was followed by monitoring the optical density at 595 nm every 15 min for up to 72 h using a Sunrise plate reader (Tecan Group). The experiment was performed with three independent strain isolates and two duplicates of each strain, but Fig. 8E,F only shows data from one representative strain analyzed in duplicate. Based on the growth curves (OD_{595} as a function of time) obtained from these experiments, an 'area under the curve' (AUC) value was derived: above OD_{595} > 0 after 72 h (total duration of the experiment); *x*-axis cutoff = 72 h; *y*-axis cutoff = 0.0. The value along the *y*-axis is in arbitrary units, but nonetheless directly reflects the growth of each strain. In Fig. 8E,F, we felt that presenting all the growth curves in the conventional manner would be confusing and impractical because of the large number of conditions and strains that were tested. Instead of conventional growth curves, we provided a visual representation that is intuitively obvious to understand. In Fig. 8E,F, the growth values are in arbitrary units obtained directly from the calculation described above using PRISM GRAPHPAD. Only raw data were involved in the calculations. There was no normalization or percentage of total growth adjustment. Any growth above OD_{595} = 0.0 for up to 72 h was calculated by the software. In this representation, the magnitude of the number is directly proportional to the extent of growth.

LC-MS/MS detection of the deuterated NAM moiety of NAD$^+$

Metabolite extracts were prepared as described below with buffered EtOH preheated at 80 °C (75% EtOH/ 25% 10 mM HEPES, pH 7.1 v/v; EtOH/HEPES) from pellets of cells exposed to 5 mM d_4-NAM for 2 h at 30 °C. The metabolite extracts were analyzed using an Agilent Q-TOF 6520 mass spectrometer equipped with a nanoelectrospray ion source. The mass spectrometer was operated in positive ion mode and scanning from *m*/*z* 110 to 200. A 5 µL aliquot of metabolite extract was applied to a custom-made C18 trapping column (4 mm length, 360 µm i.d.) that was washed for 5 min at 15 µL·min^{-1} with 0.2% (v/v) formic acid (FA). Metabolites were then eluted from the trapping column and resolved on a C18 analytical column (10 cm length, 150 µm i.d.) using a gradient from 5 to 30% (v/v) acetonitrile containing 0.2% (v/v) FA, which was applied at 600 nL·min^{-1} over 60 min.

Targeted quantitative metabolomics

Our LC-MS/MS procedure for targeted and quantitative metabolomics was designed to detect 24 analytes: NAM, NAM *N1*-oxide, *N1*-methyl NAM, *N1*-methyl-2-pyridone-5-carboxamide (2PY), *N1*-methyl-4-pyridone-5-carboxamide (4PY), NA, NR, cytidine, uridine, NaR, inosine, cytidine monophosphate, uridine monophosphate, NMN, NaMN, inosine monophosphate (IMP), ADP, ATP, ADP-ribose, nicotinic acid adenine dinucleotide (NaAD), NAD$^+$, NADH, NADP$^+$, and NADPH.

To optimize detection and quantitation, metabolites were fractionated under two types of conditions for liquid chromatography. Separation A (acidic conditions) was employed for light and heavy forms of NAM, NA, and NR, as well as four other NAM-related metabolites (NAM *N1*-oxide, *N1*-methyl NAM, 2PY, and 4PY). Separation B (basic conditions) was used for all the other metabolites mentioned above. The conditions for separation A and separation B are described below in the section titled 'LC-MS/MS and Selected Reaction Monitoring (SRM) for metabolite detection'.

Our strategy to assess the concentration of a given metabolite in *C. albicans* was to determine the number of mol of that metabolite present in a population of cells of experimentally determined volume. Cell numbers and cell volumes were obtained with a Coulter counter as described further. The number of mol of a given metabolite was determined with a procedure that was modified from our previously reported method [51]. A key component of our strategy is to establish relationships between signal intensity in the mass spectrometer and mol abundance of a specific metabolite within the high complexity pools of metabolites extracted from *C. albicans*. In order to avoid quantitation errors caused by ion suppression (the fact that the signal per mol ratio of a given metabolite can be considerably lower in a complex mixture compared with a pure sample), known amounts of heavy atom-labeled metabolites of interest were added as internal standards in each *C. albicans* sample. Most of our internal standards were generated by metabolic labeling of *S. cerevisiae* with ^{13}C-glucose. This strategy can only be used to label compounds that contain ribose moieties. For this reason, the internal standards used for separation A were either chemically synthesized [51,88] or commercially purchased. For separation A (see below), stock solutions were prepared in water and contained 100 μM d_3 *N1*-methyl-4-pyridone-5-carboxamide (4-PY), 200 μM ^{18}O NR, ^{18}O, d_3 *N1*-methyl nicotinamide (Me-NAM), 400 μM ^{18}O nicotinamide (NAM), and 400 μM d_4-NA. For separation B, heavy isotope-labeled internal standards were prepared as previously described from *S. cerevisiae* cells grown in medium in which the only source of glucose was uniformly labeled with ^{13}C ([U-$^{13}C_6$]; Cambridge Isotope Laboratories, Andover, MA, USA) [51]. Because this metabolic labeling procedure results in incorporation of ^{13}C exclusively into ribose moieties, these internal standards contain either five (nucleosides and mononucleotides) or ten ^{13}C atoms / molecule (dinucleotides).

For separation B, a nine-sample standard curve was prepared as follows. Each sample contained a mixture of all the light metabolites, each of which was present at the following concentrations: 0, 0.1, 0.2, 0.6, 2, 6, 20, 60, and 200 μM. A fixed volume of ^{13}C-labeled *S. cerevisiae* extract was added to each of the nine-point 'standard curve' of light metabolites. Four hundred microlitre of hot buffered EtOH/HEPES (see above) kept at 80 °C was added to each tube for 3 min, and the volume reduced to dryness on a Labconco Centrivap under vacuum at room temperature. The mol abundance of each ^{13}C-labeled metabolite per microliter of yeast extract was then established by comparing the LC-MS/MS signals for the ^{13}C-labeled and light metabolites present in known amounts in each sample. Because of differences in sample complexity, the degrees of ionization suppression likely differ in the above standard curve samples versus experimental samples that contain both ^{13}C-labeled internal standards and a highly complex extract of ^{12}C metabolites from *C. albicans*. However, because the ^{13}C-labeled internal standards and the ^{12}C metabolites from *C. albicans* are present in the same samples, they experience the same degree of ion suppression. Hence, it is possible to use the known mol abundance of ^{13}C-labeled internal standards (determined from the standard curve) to calculate the mol abundance of metabolites in the *C. albicans* extract. As stated earlier, heavy isotope-labeled internal standards lacking ribose (e.g., ^{18}O-NAM and d_4-NA) were obtained by chemical synthesis, rather than metabolic labeling of *S. cerevisiae*. In principle, this should circumvent the need to generate a standard curve. However, because of variability in the efficiency of incorporation of heavy atoms during chemical synthesis, the signal per mol relationship was determined, as described above, using a standard curve of light metabolites. Known amounts of ^{18}O-NAM and other heavy atom-labeled chemically synthesized internal standards were then mixed with *C. albicans* metabolite extracts prior to LC-MS/MS.

Preparation of *C. albicans* cell pellets for metabolite extraction

Unless otherwise stated, cells were grown as 6 mL cultures in SC-Niacin medium until they reached exponential phase (OD_{600} = 0.4–0.6). At that time, cells were either left untreated or continuously exposed to 5 mM light NAM or d_4-NAM for time courses of up to 2 h. At each time point, 5 mL aliquots were withdrawn for metabolite extraction. These cells were harvested by centrifugation (7500 ***g*** for 5 min at 4 °C in an Avanti JE centrifuge; Beckman Coulter, Mississauga, ON, Canada), and the culture medium was removed and cell pellets resuspended by vigorous vortexing in 10 mL ice-cold water. Cells were harvested by centrifugation (7500 ***g*** for 5 min at 4 °C in an Avanti JE instrument). A second wash of the cell pellets was performed as described above. The cell pellets were stored at −80 °C prior to metabolite extraction.

Cell numbers and cell volumes were determined for calculations of metabolite concentrations. One millilitre aliquots of the original 6 mL cultures were harvested for cell counting and sizing. The average cell size in SC-Niacin was determined to be 61 fL (range from 52 to 67 fL) using a Z2 Coulter counter.

Metabolite extraction from *C. albicans* cell pellets

Heavy atom-labeled internal standards were added to the pellets in groups of four, followed by 400 μL buffered EtOH/HEPES (see above) at 80 °C [51]. Tubes were vortexed briefly, held on ice until up to 24 samples were accumulated, vortexed at 55 °C for 3 min, and centrifuged at 4 °C for 10 min (16 100 ***g***). The supernatant was transferred to fresh tubes and solvent removed to dryness in a Centrivap. On the day of analysis, samples were reconstituted with 3% acetonitrile in 10 mM ammonium acetate. Nucleosides and nucleotides derived from cells treated with d_4-NAM showed a loss of either 1 or 2 deuterium atoms (Fig. 5). To determine whether this deuterium exchange was an artifact caused by heating during *in vitro* sample processing with buffered EtOH/HEPES at 80 °C (see above), cells were also extracted at −20 °C with either 80 : 20 (v/v) methanol/water or 40 : 40 : 20 (v/v/v) methanol/acetonitrile/water. Deuterium exchange was observed regardless of the extraction temperature or solvents used, strongly suggesting that the loss of 1 or 2 Da from nucleosides and nucleotides occurred *in vivo*.

LC-MS/MS and Selected Reaction Monitoring (SRM) for metabolite detection

Analyses were performed using a Waters TQD (Waters Corporation, Milford, MA, USA) instrument and a modified version of the published method [51]. Separation A (acidic conditions) was performed with a 2 × 100 mm, 3 μ i.d., Thermo Hypercarb column held at 60 °C. The A mobile phase was 10 mM ammonium acetate in water with 0.1% (v/v) FA, and the B mobile phase was acetonitrile containing 0.1% FA. Analytes were eluted based on a gradient beginning at 5% B for 1.8 min, linearly ramping up to 40% B at 11 min, and then rapidly ramping to 90% B at 11.3 min and holding until 13.3 min, ramping down to 5% B at 13.4 min and holding until 19.5 min. The mass spectrometer was operated in SRM mode. SRM is a sensitive and accurate approach that, even within complex samples such as metabolite extracts, can unambiguously identify specific analytes based on the relationship between the intact mass of the analyte and the masses of diagnostic fragments derived from it [51]. The precursor-to-fragment transitions that we monitored were NR (255→123); NAM (123→80); NA (124→80); Me-NAM (137→94); Me-4-py (153→136); Me-2-py (153→110); Nam oxide (139→106); ^{18}O-Nam (125→80); ^{18}O-NR (257→125); d_4-NA(128→84); ^{18}O, d_3-MeNam (142→97); d_3-Me-4-py (156→139); d_2-NR (257→125); d_3-NR (258→126); d_4-NR (259→127); d_2-NAM (125→82); d_3-NAM (126→83); and d_4-NAM (127→84). Separation B (basic conditions) was performed with a 2 × 100 mm, 3μ i.d. Thermo Hypercarb column held at 60 °C. The A mobile phase was 7.5 mM ammonium acetate in water with 0.05% NH_4OH, and the B mobile phase was acetonitrile containing 0.05% NH_4OH. Analytes were eluted based on a gradient beginning at 3% B for 1.8 min, linearly ramping up to 50% B at 14 min, ramping to 90% B at 14.1 min and holding until 16.2 min, then ramping down to 3% B at 17.1 min and holding until 22 min. The mass spectrometer was operated in SRM mode, and the monitored precursor-to-fragment transitions were NAD^+ (664→136); NADP (744→136); NaAD (665→136); NMN (335→123); NaR (256→124); ADPR (560→136); d_2-NAD^+ (666→136); d_3-NAD^+ (667→136); d_4-NAD^+ (668→136); d_2-NMN (337→125); d_3-NMN (338→126); and d_4-NMN (339→127).

Transient exposure to NAM

In order to measure intracellular metabolite concentrations after transient exposure to NAM, 44-mL cultures of each strain in SC-Niacin medium were exposed to 5 mM NAM for 7 min. Eleven millilitre was withdrawn to count cells and determine intracellular concentrations before removing NAM. The rest of the culture (33 mL) was filtered under vacuum through a 0.45μ filter [52], and the filter was washed with 200 mL PBS to remove residual NAM molecules that might be trapped in the filter or extracellular molecules adventitiously adsorbed on the surface of cells. The filtration and washes lasted ~ 2 min. The filter was then transferred into a beaker containing 33 mL of SC-Niacin medium, which is devoid of NAM. Within 1 min over a shaking platform, the vast majority of cells had dissociated from the filter. A first aliquot (11 mL) was withdrawn as soon as possible after the cells had detached from the membrane (~ 3 min after the time of filtration), and a second aliquot was withdrawn 10 min later. Cells were harvested by centrifugation, washed in 10 mL ice-cold water, and resuspended in 1 mL ice-cold water. An aliquot was kept aside to determine cell numbers and cell sizes using a Coulter counter. The rest of the cells were used to extract metabolites and determine their intracellular concentrations by LC-MS/MS.

Strains and culture conditions

Stocks of *C. albicans* strains were maintained at −80 °C in growth media containing 40% glycerol. YPD (1% yeast extract, 2% Bacto Peptone, and 2% glucose) was routinely used as rich medium; 2% agar was added for YPD agar plates. For measurements of NAD^+-related metabolite concentrations and proliferation assays, cells were grown in SC-Niacin: 0.69% w/v yeast nitrogen base without amino acids or NA (Formedium, Hunstanton, UK), 2% w/v glucose, and a mixture containing the 20 amino acids and five supplements: adenine, uracil, uridine, inositol, and para-aminobenzoic acid. In the SC-Niacin medium, the final

concentration of each amino acid and supplement was 76 mg·mL^{-1}, except for leucine, which was present at 380 mg·mL^{-1}. Because Trp precipitates over prolonged periods of time, SC-Niacin medium was prepared at most 1–2 days prior to each experiment. *Escherichia coli* DH10B or Mach1 cells were used for DNA cloning procedures. *E. coli* cells were grown in Luria–Bertani (LB) medium in which appropriate antibiotics, namely chloramphenicol (CM, 34 μg·mL^{-1}) or ampicillin (AMP, 100 μg·mL^{-1}), were added.

All the *C. albicans* strains used in this study are listed in Table 1, and the sequences of all the oligonucleotide primers used to generate those strains are listed in Table 2. *C. albicans* strains constructed using auxotrophy markers (*HIS1* or *ARG4*) were selected by growing cells in synthetic complete (SC) medium (0.67% Difco yeast nitrogen base, 2% glucose and amino acid mixtures that lacked either histidine or arginine). Selection for nourseothricin (NAT)-resistant strains was performed in the presence of 200 μg·mL^{-1} NAT (Werner BioAgents, Jena, Germany). Selection for hygromycin B (HygB)-resistant strains was conducted in the presence of 800 μg·mL^{-1} HygB [89]. For repression of the *Tet* promoter driving expression of *QNS1* (NAD^+ synthetase), an overnight culture was diluted to an optical density at 600 nm (OD_{600}) of 0.005 in fresh medium containing 20–50 μg·mL^{-1} Dox (Sigma-Aldrich, Oakville, ON, Canada) with or without 10 μM NR and cells were grown for 24 h [11,48,90].

Nicotinamidase (*pnc1*Δ/Δ) mutants

PNC1 (orf19.6684/C7_03520W_A) gene deletion cassettes were amplified by polymerase chain reaction (PCR) from pSN52 or pSN69 with fusion PCR primer sets (ST8/ST10 and ST9/ST11, Table 2). The *PNC1* gene deletion cassettes carry either the *HIS1* or *ARG4* selection markers flanked by 120-bp sequences homologous to the upstream and downstream regions of *PNC1* [11,50]. The *HIS1*-containing amplicon was transformed into *C. albicans* strain SN152 (Table 1) using minor modifications to a previously described standard transformation protocol requiring lithium acetate [11,50]. At least two independent His^+ strains were genotyped by PCR and Southern blotting, which confirmed that those strains carried a properly deleted allele of *PNC1*. These heterozygous mutant strains were transformed with the *ARG4*-containing amplicon to generate two independent *pnc1*Δ/*pnc1*Δ homozygous deletion strains that we termed CaST33 and CaST35 (Table 1).

In a so-called GRACE strain for Dox-inducible depletion of Qns1 (Qns1-GRACE, Table 1), we inserted premature stop codons in both alleles of the *PNC1* gene using a *C. albicans*-adapted CRISPR/Cas9 mutagenesis system [62]. For this purpose, a vector for production of a small guide RNA (sgRNA) that targets nucleotides 37–56 of *PNC1* was generated by annealing two 5'-end phosphorylated primers (ST272

Table 1. *Candida albicans* strains and plasmids.

Name	Genotype	Source
SN152	*URA3 / ura3*Δ*::imm*^{434} *IRO1 / iro1*Δ*::imm*^{434} *his1*::hisG / *his1*::hisG *leu2*Δ */ leu2*Δ *arg4*Δ */ arg4*Δ	[50]
*rtt109*Δ/Δ	As SN152, *rtt109*Δ *:: C. dubliniensis ARG4/ rtt109*Δ *:: C. dubliniensis HIS1*	[11]
CaST33 *pnc1*Δ/Δ #1	As SN152, *pnc1*Δ *:: C. dubliniensis ARG4 / pnc1*Δ*:: C. dubliniensis HIS1*	This study
CaST35 *pnc1*Δ/Δ #2	As SN152, *pnc1*Δ *:: C. dubliniensis ARG4 / pnc1*Δ *:: C. dubliniensis HIS1*	This study
CaRG25 *pnc1*Δ/Δ + *PNC1* #1	As CaST33, *pnc1*Δ *:: C. dubliniensis ARG4 / PNC1-FRT*	This study
CaRG28 *pnc1*Δ/Δ + *PNC1* #2	As CaST35, *pnc1*Δ *:: C. dubliniensis ARG4 / PNC1-FRT*	This study
CaRG80 *pnc1*Δ/Δ *npt1*Δ/Δ #1	As CaST35, *npt1*Δ *:: FRT / npt1*Δ *:: FRT*	This study
CaRG101 *pnc1*Δ/Δ *npt1*Δ/Δ #2	As CaST33, *npt1*Δ *:: FRT / npt1*Δ *:: FRT*	This study
CaRG115 *pnc1*Δ/Δ *nrk1*$^{CR/CR}$ #1	As CaST33, *nrk1*^{CR} */ nrk1*^{CR}	This study
CaRG117 *pnc1*Δ/Δ *nrk1*$^{CR/CR}$ #2	As CaST33, *nrk1*^{CR} */ nrk1*^{CR}	This study
CaSS1	*his3::hisG / his3::hisG leu2::tet*R-*GAL4AD-URA3 / LEU2*	
Qns1-GRACE *qns1*Δ */ tetO-QNS1*	As CaSS1, *qns1*Δ*::HIS3 / SAT1-tetO-QNS1*	[90]
CaST194 *qns1*Δ */ tetO-QNS1*	As CaSS1, *qns1*Δ*::HIS3 / HygB-tetO-QNS1*	This study
CaST207 *qns1*Δ*/ tetO-QNS1 pnc1*^{CR}*/ pnc1*^{CR}	As CaST194, *pnc1*^{CR} */ pnc1*^{CR}	This study and [90]
CaST208 *qns1*Δ */ tetO-QNS1 pnc1*^{CR}*/ pnc1*^{CR}	As CaST194, *pnc1*^{CR} */ pnc1*^{CR}	This study and [90]
CaST209 *qns1*Δ*/ tetO-QNS1 pnc1*^{CR}*/ pnc1*^{CR}	As CaST194, *pnc1*^{CR} */ pnc1*^{CR}	This study and [90]
Plasmids		
pYM70	*Candida*-adapted hygromycin B resistance gene	[89]
pV1200		[62]

Table 1. (Continued).

Name	Genotype	Source
	Solo system for *C. albicans* Cas9/sgRNA entry expression vector, which contains the *NatR* gene, and 2-kb targeting arms for the upstream and downstream regions of the *ENO1* coding region. The Eno1 protein drives expression of CaCas9. The *NatR* gene and an *Snr52-sgRNA* cassette are flanked by FRT sites, which mediate recombination when expression of the Flp recombinase is induced.	
pV1200-*PNC1* gRNA	pV1200 encoding a gRNA sequence that targets nucleotides 37 to 56 of *PNC1* (+1 is the adenine of the ATG initiator codon)	This study
pV1200-*NRK1* gRNA	pV1200 encoding a gRNA sequence that targets nucleotides 43 to 62 of *NRK1* (+1 is the adenine of the ATG initiator codon)	This study

CR: Loss-of-function allele generated using the CRISPR/Cas9 system.

and ST273, Table 2). The double-stranded DNA product was then inserted into the pV1200 plasmid digested with *Bsm*BI [62] to generate pV1200-PNC1gRNA. A DNA double-strand break repair template was generated by fusion PCR with primer pairs ST274/ST275 and ST276/ST277 (Table 2), which resulted in a 120-bp DNA fragment with the desired mutation (GGA to TGA) in the center. The repair template was also engineered to contain a mutation of the protospacer adjacent motif (PAM), a second stop codon, as well as a silent mutation that created a unique restriction site. This last feature enabled us to quickly genotype the transformants. The *QNS1*-GRACE strain CaST194 (Table 1) was cotransformed with the purified repair template (3 μg) and the sgRNA expression plasmid pV1200-PNC1gRNA linearized with *Kpn*I and *Sac*I (5–10 μg). Two independent isolates containing premature stop codons in both alleles of the *PNC1* gene (CaST207 and CaST208, Table 1) were confirmed by PCR amplification and sequencing of a DNA fragment spanning the mutation sites. To simplify reference to those strains throughout the text, we named them based on abridged versions of their genotypes (e.g.,*qns1*$^{G/\Delta}$ *pnc1*$^{CR/CR}$). The G/Δ superscript indicates that one allele of the *QNS1* gene is placed under a Dox-repressible promoter (GRACE allele), while the second allele of *QNS1* is deleted. The CR/CR superscript indicates that both alleles of the *PNC1* gene contain premature stop codons introduced by CRISPR/Cas9.

To construct a *PNC1* revertant strain (*pnc1*Δ/Δ + *PNC1*), a DNA fragment derived from a region located downstream of the *PNC1* stop codon was amplified by PCR with primer pair RG3/RG4 (Table 2) from the WT SN152 strain. This PCR product was then inserted between the *Xho*I and *Apa*I sites of plasmid pSFS2A [87,91], thus creating plasmid pPNC1$_{down}$. Next, a DNA fragment containing the *PNC1* ORF was amplified by PCR using primer pair RG1/RG2 (Table 2) and inserted between the *Sac*II and *Not*I sites of plasmid pPNC1$_{down}$, thus resulting in plasmid pPNC1$_{rev}$. The *Apa*I-*Apa*I *PNC1-SAT1* fragment derived from pPNC1$_{rev}$ was used to transform the *pnc1*Δ/Δ #1 strain (Table 1). At least two independent transformants, CaRG25 and CaRG28 (Table 1) were selected, and their genotype verified by PCR and Southern blotting.

Nicotinic acid phosphoribosyltransferase (*npt1*Δ/*npt1*Δ) null mutants

Deletion of the *NPT1* gene (orf19.7176/ C7_040440_C) in *pnc1*Δ*::ARG4* / *pnc1*Δ*::HIS1* null mutants (CaST33 and CaST35, Table 1) was achieved using the *SAT1* flipper cassette [91]. A DNA fragment spanning nucleotides +1267 to +1594 (+1 being the first nucleotide of the ATG start codon) derived from the 3′-UTR of *NPT1* was amplified by PCR using primer pair ST100/ST101. This fragment was inserted between the *Xho*I and *Apa*I sites of pSFS2A [91] to create pNTP1$_{down}$. Next, a DNA fragment corresponding to a region from −275 to −1 upstream of the *NPT1* start codon was amplified by PCR from SN152 cells with primer pair ST98/ST99. This PCR product was inserted between the *Sac*II and *Not*I sites of pNPT1$_{down}$, thus creating plasmid pNPT1$_{del}$, which contains the *SAT1* flipper cassette flanked by sequences homologous to the 5′-UTR and 3′-UTR of the *NPT1* gene. An *Apa*I-*Apa*I fragment containing *NPT1*$_{5'\text{-}UTR}$ - *SAT1 cassette* - *NPT1*$_{3'\text{-}UTR}$ was excised from pNPT1$_{del}$ and then used to transform strain *pnc1*Δ/Δ #1 (CaST33) or *pnc1*Δ/Δ #2 (CaST35). Two rounds of insertion/excision generated an *npt1*Δ/*npt1*Δ homozygous null mutation in the *pnc1*Δ/*pnc1*Δ mutant background. Two independent transformants were selected, and deletion of the two *NPT1* alleles was verified by PCR and Southern blotting (CaRG80 and CaRG101, Table 1).

Nicotinamide riboside kinase (*nrk1*$^{CR/CR}$) mutants

Disruption of the *NRK1* gene (orf19.511/ CR_04230W_A) in the *pnc1*Δ/Δ #1 strain (CaST33) was achieved using CRISPR/Cas9 to produce a *pnc1*Δ/Δ *nrk1*$^{CR/CR}$ mutant strain. The *CR* superscript represents loss-of-function alleles created using CRISPR/Cas9. A construct for

Table 2. Oligonucleotides.

Primer	Sequence (5′→3′)
ST8	5’ – CACTCCTAACCATACGCCATTATCACTAACAATCTCTTA TACTAAAAGCAAACAATAACTTGTGGAATTGTGAGCGGATA
ST9	5’ – CTCCGGAACAACACAAAAAAAAGCACGTAACGATGAATAGA GAAAATATATAAAACCTTCCACTCCTAACCATACGCCAT
ST10	5’ – CACCATTATCAATAAATAGTTTATCTGTGTCATTAATTTTCTCT GGATAAACCGATTCACGTTTTCCCAGTCACGACGTT
ST11	5’ – CATTGACCATCTCTTATTTAAATAAAGAATCAAATTTCTCAT CATTATCAACTATTGTAACACCATTATCAATAAATAGT
ST272	5’ – ATTTGATGGCCAATGATCCATTAGGG
ST273	5’ – AAAACCCTAATGGATCATTGGCCATC
ST274	5’ – ACTATGAAGAAAACAGCATTAATAGTAGTTGATCTACAAGA GGATTTCTAACAGCCTAATTGATC
ST275	5’ – TGGTTGATTTTGGGTATAACTGATCGACCATTTTTAATGGCC AATGATCAATTAGGCTGTTAGAA
ST276	5 – ACTATGAAGAAAACAGCATT
ST277	5’ – TGGTTGATTTTGGGTATAAC
RG1	5’ – TCCCCGCGGGCCCCTTAATGGACCAACTACTTTAAATT
RG2	5’ – CTAGAGCGGCCGCAGTACGGACAATCTGATAGA
RG3	5’ – ACTTCCTCGAGCTTATATTGATCTACTTTTC
RG4	5’ – GTACCGGGCCCTGATCAATTGAATGAATTAT
ST102	5’ – TTATACTTTTCAGTTACTTCATCGAATACCATTTGCCGAGG CAAGCTATAGTTATTGACCTGTGGAATTGTGAGCGGATA
ST103	5’ – CTGCCTGCTCGTGCCGAACTAGGTTTATCAAAAGTTCAACG TTTTTTTTTTATTGGCAATTTATACTTTTCAGTTACTTC
ST104	5’ – AATCACTCAACTGTTTGGTAGGGCTTACACACATTAAATT CGAATACTATACACGACCCTGTTTTCCCAGTCACGACGTT
ST105	5’ – AAAAAATGTATACTCATCTAGTCATTCCGAAAAAGAACG AAAGAAGAAGAAAAAAAAAGGAATCACTCAACTGTTTGGTA
RG32	5’ – ATTTGCTTGGTGGTGCGTCATCTTCG
RG33	5’ – AAAACGAAGATGACGCACCACCAAGC
RG48	5’ – TTTTCTAAAATGACTACTACTGGTA
RG49	5’ – TGTAAAGTAAAAGTCATCCAAATGT
ST270	5’ – TCATGAGGCGCTAACTATAGAG
ST271	5’ – CGTCAAAACTAGAGAATAATAAAG

expression of a sgRNA targeting nucleotides +43 to +62 bp (relative to the adenine of ATG at +1) of *NRK1* was generated by annealing two 5′-phosphorylated primers (RG32 and RG33) and the product inserted into the *Bsm*BI site of pV1200. A DNA repair template was generated by PCR with the primer pair RG48/RG49, which resulted in a 150-bp DNA fragment with the desired mutation (GGT to TGA) at the center. Our repair template contained a mutation of the PAM site, a stop codon, and a unique silent restriction site that enabled quick genotyping of transformants. The *pnc1*Δ/Δ #1 (CaST33) mutant strain was transformed with the guide RNA expression plasmid (linearized with *Kpn*I and *Sac*I, 5–10 μg) and the purified repair template (3 μg). The genotypes of two transformants, CaRG115 and CaRG117 (Table 1), were verified by amplifying the region containing the mutation, followed by DNA sequencing (data not shown).

Glutamine-dependent NAD^+ synthetase (*qns1* $^{G/\Delta}$) mutants

A *QNS1* conditional mutant (Qns1-GRACE; *qns1*Δ / *tetO-QNS1*) was obtained from the GRACE (gene repression and conditional expression) strain collection [90], and its genotype was verified by PCR and DNA sequencing. The GRACE collection is derived from the *C. albicans* CaSS1 strain, which expresses a fusion protein (TetR-ScGal4-AD) that consists of the DNA binding domain of the *E. coli* tetracycline-dependent repressor (TetR), fused to the *S. cerevisiae* Gal4 activation domain (ScGal4-AD). In this study, we constructed a modified *QNS1* conditional mutant strain that is compatible with the CRISPR/Cas9 Solo system by replacing the nourseothricin (NAT) resistance gene (*SAT1*) present in the GRACE collection strains with a *C. albicans*-adapted hygromycin B (*HygB*) resistance gene [89]. Primer pairs ST266/ST267 and ST268/ST269 for

fusion PCR were used to amplify the *HygB* cassette and transform Qns1-GRACE cells. HygB-resistant and NAT-sensitive transformants were selected and their genotype verified by PCR (CaST194; Table 1). In growth media containing 50 $\mu g \cdot mL^{-1}$ Dox, CaST194 failed to proliferate to the same extent as the parental strain (Qns1-GRACE).

Immunoblotting

Whole-cell lysates were prepared from two OD_{600} units of cells (20 million cells) using an alkaline method for cell lysis [92]. Proteins from whole-cell lysates were separated through SDS-15% polyacrylamide gels. This was followed by protein transfer onto nitrocellulose membranes using a semidry transfer system (Bio-Rad Laboratoris, Mississauga, ON, Canada) for 75 min at 20 V in 1× Towbin buffer (25 mM Tris, 192 mM Glycine, pH 8.3) containing 5% methanol and 0.02% w/v SDS. For immunoblots of histones, proteins were transferred to nitrocellulose membranes (0.2 µm porosity) by semidry transfer for 1 h at 10 V using 1× Towbin buffer containing 5% methanol and 0.02% SDS. To probe for H3K56 acetylation, we used an affinity-purified rabbit polyclonal antibody against H3K56ac known as AV105-GE (1 : 500 dilution) [93]. A rabbit polyclonal antibody raised against a nonmodified N-terminal peptide of H3 (AV71/72; 1 : 1000 dilution) was used to assess whether equivalent amounts of histone H3 were present in all the lanes [93].

Acknowledgements

RG and ST were recipients of Mitacs Accelerate awards. ST was also recipient of a postdoctoral fellowship from the Fonds de Recherche du Québec—Santé (FRQS). We are indebted to Eun-Hye Lee and Mohammed Alsady for technical assistance, Valmik Vyas and Gerald Fink for the *C. albicans* CRISPR/Cas9 cassette pV1200, and Brian Wong for the *C. albicans* plasmid pYM70 containing a synthetic hygromycin B resistance gene (*CaHygB*). We are grateful to Merck Sharp & Dohme for making the Grace collection available to the academic research community and Dr. Scott Walker (Merck Sharp & Dohme) for careful reading of the manuscript and insightful comments. We are grateful to Drs. Martine Raymond and Jean-Claude Labbé for their valuable suggestions regarding the experiments and the manuscript, Pierre Thibault for advice on mass spectrometry, and Frédéric Lévesque for help with retrieval of archived data. We thank Drs. Brendan Cormack, Cynthia Wolberger, and Jeffrey Smith for valuable suggestions regarding some of the experiments. Research in AV's laboratory was supported by funds from Mitacs-Merck-Université de Montréal (IT07989), the Canadian Institutes for Health Research (CIHR, FRN 125916), and the Natural Sciences and Engineering Research Council of Canada (NSERC, RGPIN-2019-05796). CB's laboratory was funded by the Roy J. Carver Trust and the Alfred E. Mann Family Foundation.

Conflict of interest

The authors declare no conflict of interest.

Author contributions

RG, ST, CB, and AV conceived and designed the experiments. RG, ST, MS, and EB performed the experiments. RG, ST, EB, MS, CB, and AV analyzed the data. RG, ST, and MS contributed reagents, materials, and analysis tools. RG, ST, CB, and AV wrote the manuscript.

Peer Review

The peer review history for this article is available at https://publons.com/publon/10.1111/febs.15622.

References

1 Pfaller MA & Diekema DJ (2010) Epidemiology of invasive mycoses in North America. *Crit Rev Microbiol* **36**, 1–53.
2 Kim J & Sudbery P (2011) *Candida albicans*, a major human fungal pathogen. *J Microbiol* **49**, 171–177.
3 Neville BA, d'Enfert C & Bougnoux ME (2015) *Candida albicans* commensalism in the gastrointestinal tract. *FEMS Yeast Res* **15**, fov081.
4 Jabra-Rizk MA, Kong EF, Tsui C, Nguyen MH, Clancy CJ, Fidel PL Jr & Noverr M (2016) *Candida albicans* Pathogenesis: fitting within the host-microbe damage response framework. *Infect Immun* **84**, 2724–2739.
5 Segal BH, Kwon-Chung J, Walsh TJ, Klein BS, Battiwalla M, Almyroudis NG, Holland SM & Romani L (2006) Immunotherapy for fungal infections. *Clin Infect Dis* **42**, 507–515.
6 Pfaller MA & Diekema DJ (2007) Epidemiology of invasive candidiasis: a persistent public health problem. *Clin Microbiol Rev* **20**, 133–163.
7 Antinori S, Milazzo L, Sollima S, Galli M & Corbellino M (2016) Candidemia and invasive candidiasis in adults: a narrative review. *Eur J Intern Med* **34**, 21–28.
8 Low CY & Rotstein C (2011) Emerging fungal infections in immunocompromised patients. *F1000 Med Rep* **3**, 14.

9 Kuchler K, Jenull S, Shivarathri R & Chauhan N (2016) Fungal KATs/KDACs: a new highway to better antifungal drugs? *PLoS Pathog* **12**, e1005938.

10 Lopes da Rosa J, Boyartchuk VL, Zhu LJ & Kaufman PD (2010) Histone acetyltransferase Rtt109 is required for *Candida albicans* pathogenesis. *Proc Natl Acad Sci USA* **107**, 1594–1599.

11 Wurtele H, Tsao S, Lepine G, Mullick A, Tremblay J, Drogaris P, Lee EH, Thibault P, Verreault A & Raymond M (2010) Modulation of histone H3 lysine 56 acetylation as an antifungal therapeutic strategy. *Nat Med* **16**, 774–780.

12 Hnisz D, Tscherner M & Kuchler K (2011) Targeting chromatin in fungal pathogens as a novel therapeutic strategy: histone modification gets infectious. *Epigenomics* **3**, 129–132.

13 Dahlin JL, Kottom T, Han J, Zhou H, Walters MA, Zhang Z & Limper AH (2014) *Pneumocystis jirovecii* Rtt109, a novel drug target for *Pneumocystis pneumonia* in immunosuppressed humans. *Antimicrob Agents Chemother* **58**, 3650–3659.

14 Nobile CJ, Fox EP, Hartooni N, Mitchell KF, Hnisz D, Andes DR, Kuchler K & Johnson AD (2014) A histone deacetylase complex mediates biofilm dispersal and drug resistance in *Candida albicans*. *MBio* **5**, e01201–01214.

15 Pfaller MA, Messer SA, Georgopapadakou N, Martell LA, Besterman JM & Diekema DJ (2009) Activity of MGCD290, a Hos2 histone deacetylase inhibitor, in combination with azole antifungals against opportunistic fungal pathogens. *J Clin Microbiol* **47**, 3797–3804.

16 Lopes da Rosa J & Kaufman PD (2013) Chromatin-mediated *Candida albicans* virulence. *Biochim Biophys Acta* **1819**, 349–355.

17 Pfaller MA, Rhomberg PR, Messer SA & Castanheira M (2015) *In vitro* activity of a Hos2 deacetylase inhibitor, MGCD290, in combination with echinocandins against echinocandin-resistant *Candida* species. *Diagn Microbiol Infect Dis* **81**, 259–263.

18 Driscoll R, Hudson A & Jackson SP (2007) Yeast Rtt109 promotes genome stability by acetylating histone H3 on lysine 56. *Science* **315**, 649–652.

19 Han J, Zhou H, Horazdovsky B, Zhang K, Xu RM & Zhang Z (2007) Rtt109 acetylates histone H3 lysine 56 and functions in DNA replication. *Science* **315**, 653–655.

20 Tsubota T, Berndsen CE, Erkmann JA, Smith CL, Yang L, Freitas MA, Denu JM & Kaufman PD (2007) Histone H3–K56 acetylation is catalyzed by histone chaperone-dependent complexes. *Mol Cell* **25**, 703–712.

21 Zhang L, Serra-Cardona A, Zhou H, Wang M, Yang N, Zhang Z & Xu RM (2018) Multisite substrate recognition in Asf1-dependent acetylation of histone H3 K56 by Rtt109. *Cell* **174**, 818–830.

22 Celic I, Masumoto H, Griffith WP, Meluh P, Cotter RJ, Boeke JD & Verreault A (2006) The sirtuins Hst3 and Hst4p preserve genome integrity by controlling histone H3 lysine 56 deacetylation. *Curr Biol* **16**, 1280–1289.

23 Maas NL, Miller KM, DeFazio LG & Toczyski DP (2006) Cell cycle and checkpoint regulation of histone H3 K56 acetylation by Hst3 and Hst4. *Mol Cell* **23**, 109–119.

24 Thaminy S, Newcomb B, Kim J, Gatbonton T, Foss E, Simon J & Bedalov A (2007) Hst3 is regulated by Mec1-dependent proteolysis and controls the S phase checkpoint and sister chromatid cohesion by deacetylating histone H3 at lysine 56. *J Biol Chem* **282**, 37805–37814.

25 Hachinohe M, Hanaoka F & Masumoto H (2011) Hst3 and Hst4 histone deacetylases regulate replicative lifespan by preventing genome instability in *Saccharomyces cerevisiae*. *Genes Cells* **16**, 467–477.

26 Chaabane F, Graf A, Jequier L & Coste AT (2019) Review on antifungal resistance mechanisms in the emerging pathogen *Candida auris*. *Front Microbiol* **10**, 2788.

27 Dahlin JL, Sinville R, Solberg J, Zhou H, Han J, Francis S, Strasser JM, John K, Hook DJ, Walters MA *et al.* (2013) A cell-free fluorometric high-throughput screen for inhibitors of Rtt109-catalyzed histone acetylation. *PLoS One* **8**, e78877.

28 Lopes da Rosa J, Bajaj V, Spoonamore J & Kaufman PD (2013) A small molecule inhibitor of fungal histone acetyltransferase Rtt109. *Bioorg Med Chem Lett* **23**, 2853–2859.

29 Landry J, Slama JT & Sternglanz R (2000) Role of NAD(+) in the deacetylase activity of the Sir2-like proteins. *Biochem Biophys Res Commun* **278**, 685–690.

30 Jackson MD, Schmidt MT, Oppenheimer NJ & Denu JM (2003) Mechanism of nicotinamide inhibition and transglycosidation by Sir2 histone/protein deacetylases. *J Biol Chem* **278**, 50985–50998.

31 Sauve AA & Schramm VL (2003) Sir2 regulation by nicotinamide results from switching between base exchange and deacetylation chemistry. *Biochemistry* **42**, 9249–9256.

32 Chapman SW, Sullivan DC & Cleary JD (2008) In search of the holy grail of antifungal therapy. *Trans Am Clin Climatol Assoc* **119**, 197–215.

33 Knip M, Douek IF, Moore WP, Gillmor HA, McLean AE, Bingley PJ, Gale EA & European Nicotinamide Diabetes Intervention Trial Group (2000) Safety of high-dose nicotinamide: a review. *Diabetologia* **43**, 1337–1345.

34 MacKay D, Hathcock J & Guarneri E (2012) Niacin: chemical forms, bioavailability, and health effects. *Nutr Rev* **70**, 357–366.

35 Lenglet A, Liabeuf S, Guffroy P, Fournier A, Brazier M & Massy ZA (2013) Use of nicotinamide to treat

hyperphosphatemia in dialysis patients. *Drugs R D* **13**, 165–173.
36 Libri V, Yandim C, Athanasopoulos S, Loyse N, Natisvili T, Law PP, Chan PK, Mohammad T, Mauri M, Tam KT *et al.* (2014) Epigenetic and neurological effects and safety of high-dose nicotinamide in patients with Friedreich's ataxia: an exploratory, open-label, dose-escalation study. *Lancet* **384**, 504–513.
37 Bogan KL & Brenner C (2008) Nicotinic acid, nicotinamide, and nicotinamide riboside: a molecular evaluation of NAD^+ precursor vitamins in human nutrition. *Annu Rev Nutr* **28**, 115–130.
38 Horsman MR, Hoyer M, Honess DJ, Dennis IF & Overgaard J (1993) Nicotinamide pharmacokinetics in humans and mice: a comparative assessment and the implications for radiotherapy. *Radiother Oncol* **27**, 131–139.
39 Dragovic J, Kim SH, Brown SL & Kim JH (1995) Nicotinamide pharmacokinetics in patients. *Radiother Oncol* **36**, 225–228.
40 Stratford MR, Dennis MF, Hoskin P, Phillips H, Hodgkiss RJ & Rojas A (1996) Nicotinamide pharmacokinetics in humans: effect of gastric acid inhibition, comparison of rectal vs oral administration and the use of saliva for drug monitoring. *Br J Cancer* **74**, 16–21.
41 Bernier J, Stratford MR, Denekamp J, Dennis MF, Bieri S, Hagen F, Kocagoncu O, Bolla M & Rojas A (1998) Pharmacokinetics of nicotinamide in cancer patients treated with accelerated radiotherapy: the experience of the Co-operative Group of Radiotherapy of the European Organization for Research and Treatment of Cancer. *Radiother Oncol* **48**, 123–133.
42 Preiss J & Handler P (1958) Biosynthesis of diphosphopyridine nucleotide. II. Enzymatic aspects. *J Biol Chem* **233**, 493–500.
43 Ghislain M, Talla E & Francois JM (2002) Identification and functional analysis of the *Saccharomyces cerevisiae* nicotinamidase gene, *PNC1*. *Yeast* **19**, 215–224.
44 Ma B, Pan SJ, Zupancic ML & Cormack BP (2007) Assimilation of NAD(+) precursors in *Candida glabrata*. *Mol Microbiol* **66**, 14–25.
45 Gossmann TI, Ziegler M, Puntervoll P, de Figueiredo LF, Schuster S & Heiland I (2012) NAD(+) biosynthesis and salvage–a phylogenetic perspective. *FEBS J* **279**, 3355–3363.
46 Chaffin WL, Barton RA, Jacobson EL & Jacobson MK (1979) Nicotinamide adenine dinucleotide metabolism in *Candida albicans*. *J Bacteriol* **139**, 883–888.
47 Wogulis M, Chew ER, Donohoue PD & Wilson DK (2008) Identification of formyl kynurenine formamidase and kynurenine aminotransferase from *Saccharomyces cerevisiae* using crystallographic, bioinformatic and biochemical evidence. *Biochemistry* **47**, 1608–1621.
48 Bieganowski P & Brenner C (2004) Discoveries of nicotinamide riboside as a nutrient and conserved NRK genes establish a Preiss-Handler independent route to NAD^+ in fungi and humans. *Cell* **117**, 495–502.
49 Smith BC, Anderson MA, Hoadley KA, Keck JL, Cleland WW & Denu JM (2012) Structural and kinetic isotope effect studies of nicotinamidase (Pnc1) from *Saccharomyces cerevisiae*. *Biochemistry* **51**, 243–256.
50 Noble SM & Johnson AD (2005) Strains and strategies for large-scale gene deletion studies of the diploid human fungal pathogen *Candida albicans*. *Eukaryot Cell* **4**, 298–309.
51 Trammell SA & Brenner C (2013) Targeted, LCMS-based metabolomics for quantitative measurement of NAD(+) metabolites. *Comput Struct Biotechnol J* **4**, e201301012.
52 Han TL, Cannon RD & Villas-Boas SG (2012) The metabolic response of *Candida albicans* to farnesol under hyphae-inducing conditions. *FEMS Yeast Res* **12**, 879–889.
53 San Pietro A (1955) Base-catalyzed deuterium exchange with diphosphopyridine nucleotide. *J Biol Chem* **217**, 589–593.
54 Zoltewicz JA & Helmick LS (1970) Base-catalyzed hydrogen-deuterium exchange of N-substituted pyridinium ions. Inductive effects and internal return. *J Am Chem Soc* **92**, 7547–7552.
55 Anderson RM, Bitterman KJ, Wood JG, Medvedik O, Cohen H, Lin SS, Manchester JK, Gordon JI & Sinclair DA (2002) Manipulation of a nuclear NAD^+ salvage pathway delays aging without altering steady-state NAD^+ levels. *J Biol Chem* **277**, 18881–18890.
56 Sorci L, Blaby I, De Ingeniis J, Gerdes S, Raffaelli N, de Crecy Lagard V & Osterman A (2010) Genomics-driven reconstruction of *Acinetobacter* NAD metabolism: insights for antibacterial target selection. *J Biol Chem* **285**, 39490–39499.
57 Natalini P, Ruggieri S, Raffaelli N & Magni G (1986) Nicotinamide mononucleotide adenylyltransferase. Molecular and enzymatic properties of the homogeneous enzyme from baker's yeast. *Biochemistry* **25**, 3725–3729.
58 Zhou T, Kurnasov O, Tomchick DR, Binns DD, Grishin NV, Marquez VE, Osterman AL & Zhang H (2002) Structure of human nicotinamide/nicotinic acid mononucleotide adenylyltransferase. Basis for the dual substrate specificity and activation of the oncolytic agent tiazofurin. *J Biol Chem* **277**, 13148–13154.
59 Kato M & Lin SJ (2014) *YCL047C/POF1* is a novel nicotinamide mononucleotide adenylyltransferase (NMNAT) in *Saccharomyces cerevisiae*. *J Biol Chem* **289**, 15577–15587.

60 Tempel W, Rabeh WM, Bogan KL, Belenky P, Wojcik M, Seidle HF, Nedyalkova L, Yang T, Sauve AA, Park HW *et al*. (2007) Nicotinamide riboside kinase structures reveal new pathways to NAD^+. *PLoS Biol* **5**, e263.
61 Belenky P, Racette FG, Bogan KL, McClure JM, Smith JS & Brenner C (2007) Nicotinamide riboside promotes Sir2 silencing and extends lifespan via Nrk and Urh1/Pnp1/Meu1 pathways to NAD^+. *Cell* **129**, 473–484.
62 Vyas VK, Barrasa MI & Fink GR (2015) A *Candida albicans* CRISPR system permits genetic engineering of essential genes and gene families. *Sci Adv* **1**, e1500248.
63 Imai S, Armstrong CM, Kaeberlein M & Guarente L (2000) Transcriptional silencing and longevity protein Sir2 is an NAD-dependent histone deacetylase. *Nature* **403**, 795–800.
64 Smith JS, Brachmann CB, Celic I, Kenna MA, Muhammad S, Starai VJ, Avalos JL, Escalante-Semerena JC, Grubmeyer C, Wolberger C *et al*. (2000) A phylogenetically conserved NAD^+-dependent protein deacetylase activity in the Sir2 protein family. *Proc Natl Acad Sci USA* **97**, 6658–6663.
65 Tanner KG, Landry J, Sternglanz R & Denu JM (2000) Silent information regulator 2 family of NAD-dependent histone/protein deacetylases generates a unique product, 1-O-acetyl-ADP-ribose. *Proc Natl Acad Sci USA* **97**, 14178–14182.
66 Sauve AA, Celic I, Avalos J, Deng H, Boeke JD & Schramm VL (2001) Chemistry of gene silencing: the mechanism of NAD^+-dependent deacetylation reactions. *Biochemistry* **40**, 15456–15463.
67 Hoff KG, Avalos JL, Sens K & Wolberger C (2006) Insights into the sirtuin mechanism from ternary complexes containing NAD^+ and acetylated peptide. *Structure* **14**, 1231–1240.
68 Smith BC & Denu JM (2006) Sir2 protein deacetylases: evidence for chemical intermediates and functions of a conserved histidine. *Biochemistry* **45**, 272–282.
69 Hawse WF, Hoff KG, Fatkins DG, Daines A, Zubkova OV, Schramm VL, Zheng W & Wolberger C (2008) Structural insights into intermediate steps in the Sir2 deacetylation reaction. *Structure* **16**, 1368–1377.
70 Sauve AA, Moir RD, Schramm VL & Willis IM (2005) Chemical activation of Sir2-dependent silencing by relief of nicotinamide inhibition. *Mol Cell* **17**, 595–601.
71 McClure JM, Wierman MB, Maqani N & Smith JS (2012) Isonicotinamide enhances Sir2 protein-mediated silencing and longevity in yeast by raising intracellular NAD^+ concentration. *J Biol Chem* **287**, 20957–20966.
72 Kornberg A (1948) The participation of inorganic pyrophosphate in the reversible enzymatic synthesis of diphosphopyridine nucleotide. *J Biol Chem* **176**, 1475.
73 Kornberg A & Baker TA (1991) DNA Replication, 2nd edn, pp. 68–69. W.H. Freeman and Company, New York, NY.
74 Fernandez-Arenas E, Cabezon V, Bermejo C, Arroyo J, Nombela C, Diez-Orejas R & Gil C (2007) Integrated proteomics and genomics strategies bring new insight into *Candida albicans* response upon macrophage interaction. *Mol Cell Proteomics* **6**, 460–478.
75 Kusch H, Engelmann S, Bode R, Albrecht D, Morschhauser J & Hecker M (2008) A proteomic view of *Candida albicans* yeast cell metabolism in exponential and stationary growth phases. *Int J Med Microbiol* **298**, 291–318.
76 Walker GM & White NA (2017) Introduction to fungal physiology. In Fungi: Biology and Applications (Kavanagh K, ed), pp. 1–34. Wiley Online Library, Hoboken, NJ, USA.
77 Yang NJ & Hinner MJ (2015) Getting across the cell membrane: an overview for small molecules, peptides, and proteins. *Methods Mol Biol* **1266**, 29–53.
78 Kr A, Shah AH & Prasad R (2016) MFS transporters of *Candida* species and their role in clinical drug resistance. *FEMS Yeast Res* **16**.
79 Bitterman KJ, Anderson RM, Cohen HY, Latorre-Esteves M & Sinclair DA (2002) Inhibition of silencing and accelerated aging by nicotinamide, a putative negative regulator of yeast Sir2 and human SIRT1. *J Biol Chem* **277**, 45099–45107.
80 Gazanion E, Vergnes B, Seveno M, Garcia D, Oury B, Ait-Oudhia K, Ouaissi A & Sereno D (2011) *In vitro* activity of nicotinamide/antileishmanial drug combinations. *Parasitol Int* **60**, 19–24.
81 Tyers M & Wright GD (2019) Drug combinations: a strategy to extend the life of antibiotics in the 21st century. *Nat Rev Microbiol* **17**, 141–155.
82 Larkin E, Hager C, Chandra J, Mukherjee PK, Retuerto M, Salem I, Long L, Isham N, Kovanda L, Borroto-Esoda K *et al*. (2017) The Emerging pathogen *Candida auris*: growth phenotype, virulence factors, activity of antifungals, and effect of SCY-078, a novel glucan synthesis inhibitor, on growth morphology and biofilm formation. *Antimicrob Agents Chemother* **61**, e02396-16.
83 Sender R, Fuchs S & Milo R (2016) Revised estimates for the number of human and bacterial cells in the body. *PLoS Biol* **14**, e1002533.
84 Backhed F, Ley RE, Sonnenburg JL, Peterson DA & Gordon JI (2005) Host-bacterial mutualism in the human intestine. *Science* **307**, 1915–1920.
85 Enright EF, Gahan CG, Joyce SA & Griffin BT (2016) The impact of the gut microbiota on drug metabolism and clinical outcome. *Yale J Biol Med* **89**, 375–382.
86 Helmink BA, Khan MAW, Hermann A, Gopalakrishnan V & Wargo JA (2019) The microbiome, cancer, and cancer therapy. *Nat Med* **25**, 377–388.

87 Tsao S, Weber S, Cameron C, Nehme D, Ahmadzadeh E & Raymond M (2016) Positive regulation of the *Candida albicans* multidrug efflux pump Cdr1p function by phosphorylation of its N-terminal extension. *J Antimicrob Chemother* **71**, 3125–3134.
88 Yang T, Chan NY-K & Sauve AA (2007) Effective agents for increasing nicotinamide adenine dinucleotide concentrations in mammalian cells. *J Med Chem* **50**, 6458–6461.
89 Basso LR Jr, Bartiss A, Mao Y, Gast CE, Coelho PS, Snyder M & Wong B (2010) Transformation of *Candida albicans* with a synthetic hygromycin B resistance gene. *Yeast* **27**, 1039–1048.
90 Roemer T, Jiang B, Davison J, Ketela T, Veillette K, Breton A, Tandia F, Linteau A, Sillaots S, Marta C *et al.* (2003) Large-scale essential gene identification in *Candida albicans* and applications to antifungal drug discovery. *Mol Microbiol* **50**, 167–181.
91 Reuss O, Vik A, Kolter R & Morschhauser J (2004) The *SAT1* flipper, an optimized tool for gene disruption in *Candida albicans*. *Gene* **341**, 119–127.
92 Kushnirov VV (2000) Rapid and reliable protein extraction from yeast. *Yeast* **16**, 857–860.
93 Masumoto H, Hawke D, Kobayashi R & Verreault A (2005) A role for cell-cycle-regulated histone H3 lysine 56 acetylation in the DNA damage response. *Nature* **436**, 294–298.
94 Robert X & Gouet P (2014) Deciphering key features in protein structures with the new ENDscript server. *Nucleic Acids Res* **42**, W320–324.

Supporting information

Additional supporting information may be found online in the Supporting Information section at the end of the article.

Table S1. Results for Fig. 3A; sensitivity to supraphysiological NAM concentrations (3 biological replicates per strain, N1 to N3).

Table S2. Results for Fig. 5B; sensitivity to supraphysiological NAM concentrations (3 biological replicates per strain, N1 to N3).

Table S3. Results for Fig. 7A; Sensitivity to supraphysiological NAM concentrations (3 biological replicates per strain, N1 to N3).

Table S4. Results for Fig. 3B; Sensitivity to moderate NAM concentrations (3 biological replicates per strain, N1 to N3).

Table S5. Results for Fig. 3C; sensitivity to MMS (6 biological replicates per strain, N1 to N6).